Supplemental Material

1 Image Preprocessing and Annotation

The raw data consisted of desensitized MP4 format fetal four-chamber view video files exported from ultrasound machines. Approximately 30 to 60 frames were extracted from each original fetal heart video and stored in JPEG format.Six ultrasound physicians with 5 to 8 years of experience were involved in the annotation of fetal four-chamber view images. Using the open-source tool LabelImg (version 2.0), they annotated the anatomical structures (left ventricle, left atrium, right ventricle, right atrium, apex, mitral valve, foramen ovale, interventricular septum, etc.) with the smallest possible rectangular bounding boxes to train the model to identify the standard four-chamber heart view. Additionally, a self-developed polygonal annotation tool was used to outline the actual boundaries of the anatomical structures to train the model for segmenting these structures, which is essential for calculating cardiac function parameters. During polygonal annotation, the tool provided playback and rewind functions, allowing the annotators to view the preceding and following frames of the annotated frame to assist in accurately identifying the boundaries of anatomical structures that may shift in position within the video, ensuring the accuracy of the annotations. After the initial annotation, two ultrasound physicians with over 10 years of experience reviewed and corrected any inaccurate bounding boxes and polygonal annotations. The reviewed and approved data were then used for training and fine-tuning the deep learning model.

2 Data Augmentation

To enhance the model's generalization ability for complex scenarios, data augmentation was implemented in offline and online parts:

For offline data augmentation, the operation includes (1) Random Scaling: Using a base scaling ratio of 0.3, the scale distribution of the input images was dynamically adjusted to force the model to learn robust feature representations for multi-scale targets. (2) Random Rotation: Images were rotated within a continuous range of angles to enhance the model's adaptability to directional changes of the target, reducing detection bias caused by viewpoint differences. (3) Random Contrast Adjustment: By dynamically adjusting the difference between the bright and dark areas of the images, the visual features under varying brightness conditions were simulated to improve the model's robustness to changes in image brightness.

For online data augmentation, a combination of multi-dimensional geometric transformations and color space perturbations was applied, including (1) Geometric Transformation Enhancement: A composite transformation involving random cropping (30% amplitude in all directions), scaling (0.5 to 1.5 times), translation, and rotation ($-15°$ to $+15°$) was used to simulate the multi-scale spatial distribution characteristics of the target in real-world scenarios. This strategy, through parametric random perturbation, forced the model to learn the feature representations of targets from different viewpoints and scales, alleviating overfitting caused by a single viewpoint. (2) Color Space Perturbation Module: The RandomDistort technique was employed to decouple multi-dimensional color features, including: non-linear perturbation in the HSV space: hue shift ($\pm$30%), saturation adjustment ($\pm$50%), and brightness fluctuation ($\pm$30%); random permutation of RGB channels with a 0.5 probability, the order of the three channels was swapped to break the inherent correlation of color features. This module simulated different imaging environments to enhance the model's detection robustness under low-contrast and color-biased conditions. (3) Target Integrity Protection Mechanism: A two-stage adaptive sampling strategy was introduced: random expansion with a 0.5 probability, the image was randomly expanded to 1.0 to 4.0 times its size to simulate the presence of the target in different backgrounds; target-aware cropping when cropping resulted in a target box area loss exceeding 50%, a hard negative sample filtering mechanism was triggered to ensure the semantic integrity of the effective target during training, preventing the model from producing erroneous detection results due to overconfidence.

After undergoing the above augmentation techniques, the images were resized to a 640x640 pixel resolution while maintaining the aspect ratio for model training.

3 Model Input and Output

The common human-based workflow for performing fetal cardiac measurement consists of a sequence of steps: (1) identifying a sequence that smoothly displays the standard fetal four-chamber view from the whole screening video; (2) determining the systolic and diastolic phase; (3) manually segmenting and drawing annotations on frames to outline cardiac chambers; and (4) manually referring to standard reference guidelines to calculate the measurement by geometric information of the annotated object, such as area or length. The above data pipeline is executed in sequence, which makes the evaluation of fetal heart function parameters inefficient and manual analysis time-consuming. Furthermore, the limited processing capacity of human operators merely support to focus on a few frames at once. The selection of measurement frames and endpoint positions involves significant subjectivity, leading to poor repeatability of measurements and even failure to replicate results in regions lacking expert resources.

To solve these problem, our AI workflow unifies these steps by a identify first and judge later way. The motivation is to shift the analysis of fetal echocardiography from the selection of key frames to the direct selection of key cardiac structures. The powerful computational capabilities of AI enable parallel analysis of every frame in fetal electrocardiograms, efficiently detecting and delineating potential anatomical boundaries. This significantly enhances data processing efficiency, thereby reducing

evaluation time for fetal cardiac function. Furthermore, the integration of the holistic analysis with the expert knowledge allows the objective automated selection of optimal measurement windows, improving the reproducibility of cardiac function assessments.Most importantly, the powerful learning capacity of AI enables recognizing visual features in complex fetal positions through extensive training with expert-collected and -annotated data. This ensures high-quality structural detection and precise boundary delineation. To this end, the AI workflow automates the entire process without the need for human intervention, greatly improving the efficiency and repeatability of fetal cardiac function evaluation.

4 RT-DETR Detector

In the identification process, the AI workflow rapidly analyses each frame of videos stored on the digital imaging and communications in medicine (DICOM) files of the patient examination and outline the visual structure that is familiar with the cardiac structure of interest. We trained a famous deep learning-based detector named RT-DETR, which combines the advantages of convolution nerual network (CNN) and Transformer. RT-DETR is specifically designed to account for the distinctive characteristics of fetal echocardiography, aiming to enhance accuracy while reducing computational cost. Segmenting fetal cardiac chambers requires capturing global structural information to guide feature extraction within locally similar blood-flow regions. Moreover, due to ultrasound image noise and the relatively large size of the cardiac chambers, there is no need to extract the extremely fine-grained local features required for natural images. RT-DETR employs a Transformer only on the smallest-scale feature map to extract global context. It then uses a lightweight feature pyramid to propagate this global information across all scales, generating uniformly sized feature blocks. Thus, RT-DETR effectively integrates global and local information within a compact architecture while significantly reducing the computational overhead associated with Transformers. The architecture retains convolutional neural network as the backbone network (using ResNet18 as the convolutional neural network backbone) to perform initial feature extraction on the input image, generating several two-dimensional feature maps. This step maps the image to a unified expression space and performs downsampling to reduce computational load before feeding it into the main Transformer module to complete the detection task. To meet the GPU memory requirements for Transformer training, a server with two RTX 4090 graphics cards was used for training, with approximately 200 rounds of convergence and early termination of training after about 3 days. When a fetal four-chamber heart ultrasound image is input into the model, the model outputs the detection boxes and structure labels for all key structures in the section, as shown in Fig. S1.

The loss function contains two parts: (1) Classification Loss:

$$\mathcal{L}_{cls} = -\Sigma_{i=1}^{N}[\hat{y}_i log(p_i) + (1-\hat{y}_i) log(1-p_i)], \tag{1}$$

where $\hat{y}_i$ and p_i denotes the ground true and predicted category, and N is the box number. (2) Bounding Box Regression Loss:

$$\mathcal{L}_{box} = \lambda_1 \Sigma_{i=1}^{4} |b_{pred}^{i} - b_{gt}^{i}| + \lambda_2 (1 - GIoU(b_{pred}, b_{gt})), \tag{2}$$

where b_{pred} and b_{gt} denote the center coordinates, width, and height of the predicted and ground-truth box, and $GIoU(\cdot)$ measures the overlap between the predicted box and the ground-truth box, addressing the issue of gradient disappearance in traditional IoU when there is no overlap.

5 Mask-Dino Segmentation Head

We designed a segmentation head to extend RT-DETR, which enables the unified Transformer-based decoding for both the object detection and segmentation tasks. The algorithm inherits most of the improvements from RT-DETR, such as cross attention with anchor box guidance, query selection, and noise reduction training. Therefore, the detection and segmentation tasks can help each other by leveraging shared intermediate features to complete both detection and boundary delineation. The segmentation head reuses the front-end backbone network, adding only about 6-8 ms to the inference time to achieve high-precision real-time detection of cardiac function. During training, the loss is calculated only for the annotated four chambers, cardiac outline, and related structures (since bounding box target detection and instance segmentation have different numbers of annotated objects), thereby enabling joint training of the detection head and segmentation head. The model was trained on a dual RTX 4090 server for 3 days, with approximately 200 rounds of training before termination. The segmentation results of the fetal cardiac ultrasound images by the AI model are shown in Fig. S2.

The loss function contains two parts: (1) Segmentation Loss:

$$\mathcal{L}_{seg} = -\Sigma_{i=1,j=1}^{H,W} [\hat{y}_{i,j} log(p_{i,j}) + (1 - \hat{y}_{i,j}) log(1 - p_{i,j})], \tag{3}$$

where $\hat{y}_i$ and p_i denotes the ground true and predicted label at the position (i, j), and H, W is the height and weight of the image. (2) Dice Loss:

$$\mathcal{L}_{dice} = 1 - \frac{2\Sigma_{i=1,j=1}^{H,W} \; p_{i,j} \; \hat{y}_{i,j}}{\Sigma_{i=1,j=1}^{H,W} p_{i,j} + \Sigma_{i=1,j=1}^{H,W} \hat{y}_{i,j}}, \tag{4}$$

In summary, the total loss function is formulated as:

$$\mathcal{L}_{loss} = \lambda_{cls}\mathcal{L}_{cls} + \lambda_{box}\mathcal{L}_{box} + \lambda_{seg}\mathcal{L}_{seg} + \lambda_{dice}\mathcal{L}_{dice}, \tag{5}$$

where the factors for each term are set as $\lambda_{cls} = 4$, $\lambda_{box} = 2$, $\lambda_{seg} = 5$, $\lambda_{dice} = 5$. Both the detection and segmentation head are based on the DETR architecture, and the segmentation task can be regarded as a more refined object detection task. Therefore, the same hyperparameters are used for both, with the difference lying in the different

loss functions used and the additional segmentation head in the segmentation model. The training hyperparameters for the detection and segmentation networks are shown in Table S1.

6 Geometric Calculation of Cardiac Function Parameters

Based on the bounding boxes and polygonal contours of the fetal cardiac structures output by the AI model, cardiac function parameters are calculated using geometric, mathematical, and image processing methods. For example, the calculation of cardiac transverse diameter requires determining two geometric endpoints through geometric methods and calculating the distance between them. Each measurement item is obtained through a similar calculation process. The cardiac cycle is calculated based on continuous video frames. The calculation of the cardiac cycle relies on the accurate segmentation of the four chambers by the segmentation head, identifying the key frames of systole and diastole through the dynamic and regular area changes, and finally estimating the fetal cardiac cycle based on these key frames. Since stored images and real-time ultrasound examination videos often contain more than one complete cardiac cycle, the model calculates the measurement values for each complete cardiac cycle in real-time and designs a strategy based on section standard and image quality assessment to determine the optimal cardiac cycle, approximating the optimal judgment standard of ultrasound physicians. The fetal cardiac function parameters measured in the four-chamber heart section using the AI model are listed in Table S2 and S3.

7 Supplemental Experiment Result

Table S1 lists the hardware configuration of the model testing. Table S4 presents the results of five state-of-the-art models and our RT-DERT on the full validation data. Also, the significance test was conducted to verify the Dice metric differences between these five methods and our approach. Fig. S3 shows two cases of the segmentation and measurement results. The segmentation errors primarily arise from two sources: global boundary shifts, and locally ambiguous boundaries, particularly between cardiac chambers and valves during valve opening. Such global shifts do not introduce substantial errors in the final measurements because endpoint errors in measurement points are often consistent in direction and thus tend to cancel each other out in the final calculation. Furthermore, cardiac chamber measurements are prioritized at end-diastole—when valves are clearly closed, therefore visualized—the impact of segmentation uncertainty on the final measurements is further minimized. The human-machine measurement results are listed in Table S5-S8. Fig. S4-S6 show the Bland-Altman graphs for global sphericity index, fractional area change of right ventricle, and ejection fraction of left ventricle in the normal dataset. Fig. S7-S9 show the Bland-Altman graphs for these parameters in the abnormal dataset.

8 Detail of Z-score modeling

Various cardiac parameters exhibit changes throughout the biparietal diameter (BPD), head circumference (HC), abdominal circumference(AC), femur length (FL), estimated fetal weight (EFW) and Last menstrual period gestational age (LMP_GA); Ultrasound mean gestational age (US_MGA). The independent variable (X) is continuous and not fixed. To establish normal reference values for fetal heart parameters, a Z score methodology for the automatic measurement of these parameters was developed.

This study continuously collects data from over 1385 singleton fetuses, with gestational age determined through early pregnancy ultrasound examinations conducted between 18w+0d weeks and 37w+6d weeks. The dataset includes only those cases that provide a complete view of the fetal four-chamber view and excludes any instances of cardiac structural abnormalities, discrepancies in gestational age, or factors that may influence fetal heart rate, such as functional extracardiac and maternal factors. Importantly, this dataset does not overlap with the data used for model building, which includes training, tuning, and validation sets. In cases where multiple four-chamber cardiac videos of the same fetus were obtained at different gestational ages, only the video with the highest image quality was retained. After adjusting gestational age based on early pregnancy ultrasound findings, 95% of independent variables—BPD, HC, AC, FL, and EFW—that exceeded the normal range on both sides were excluded, utilizing criteria published by Hadlock to construct reference ranges for fetal biometric measurements. The criteria for video collection of the four-chamber view remained consistent throughout the study. The steps to calculate Z scores and percentiles are as follows:

Step 1: Model the mean of Y (cardiac parameters) as a function of X (the clinical gestational age, ultrasound mean gestational age, BPD, HC, AC, FL, EFW). After the scatter plot was displayed, fractional polynomials were used to evaluate the specific time reference range that has been applied to fetal bioassays. The NCSS11 software program was used to analyze the sample data automatically. 44 equations arranged in descending order of R^2 values are obtained as show in Table S9.

Step 2: Derive the regression equation of standard deviation by fitting a polynomial of degree, denoted as $(SD = C0 + C1 \times X)$.

Step 3: Test the goodness of fit of the model by first considering the values of the higher R^2 or F statistics. Check whether Z-scores are normally distributed by observing the normal probability plot of Z-scores and the results of the normality test.

Step 4: The equation of Z-Score is obtained by using mean regression equation and standard deviation regression equation, denoted as:

$$Z\_score = \frac{I_{measure} - M_{normal}}{SD_{normal}}, \tag{6}$$

where, $I_{measure}$ is individual measurement, M_{normal} is predicted mean of the measurement from a normally distributed population, and SD_{normal} is standard deviation of the measurement from a normally distributed population.

Table S10-S12 shows the most regression function of the Z-score modeling for cardiac parameters of full, left and right heart, respecitively.

Vedio S1: Demonstration of the process of the automated cardiac function measurement on a normal fetus. The red box highlights key information displayed on the user interface. At the beginning of the video, the user interface displays real-time detection and segmentation results of cardiac structures. After comprehensive evaluation of the detection results, the AI determines that the current video shows a standard four-chamber heart view. Subsequently, by tracking structural changes during several cardiac cycles, it automatically selects the optimal results for cardiac function calculations.

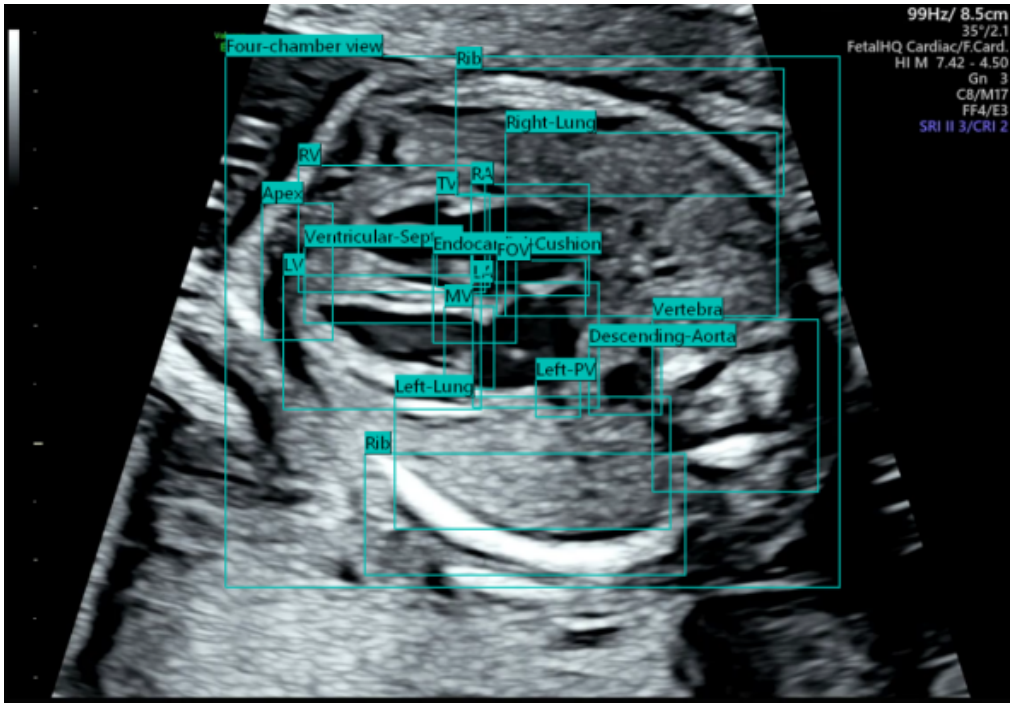

Fig. S1: The detection network's recognition of the anatomical structures

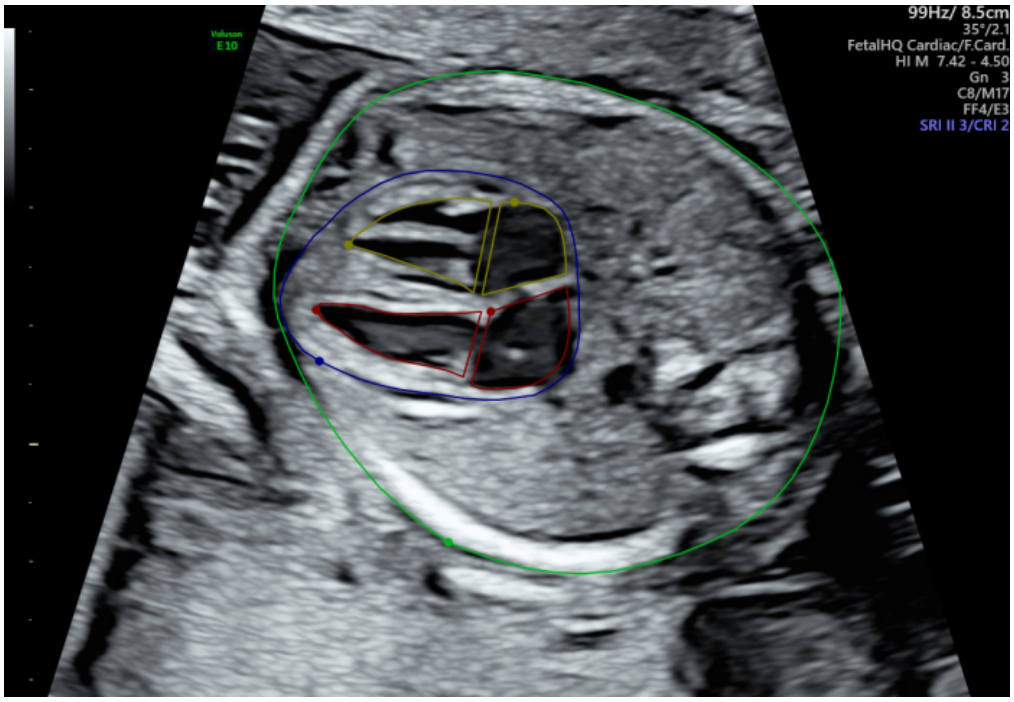

Fig. S2: An segmentation example of the Mask-Dino Head

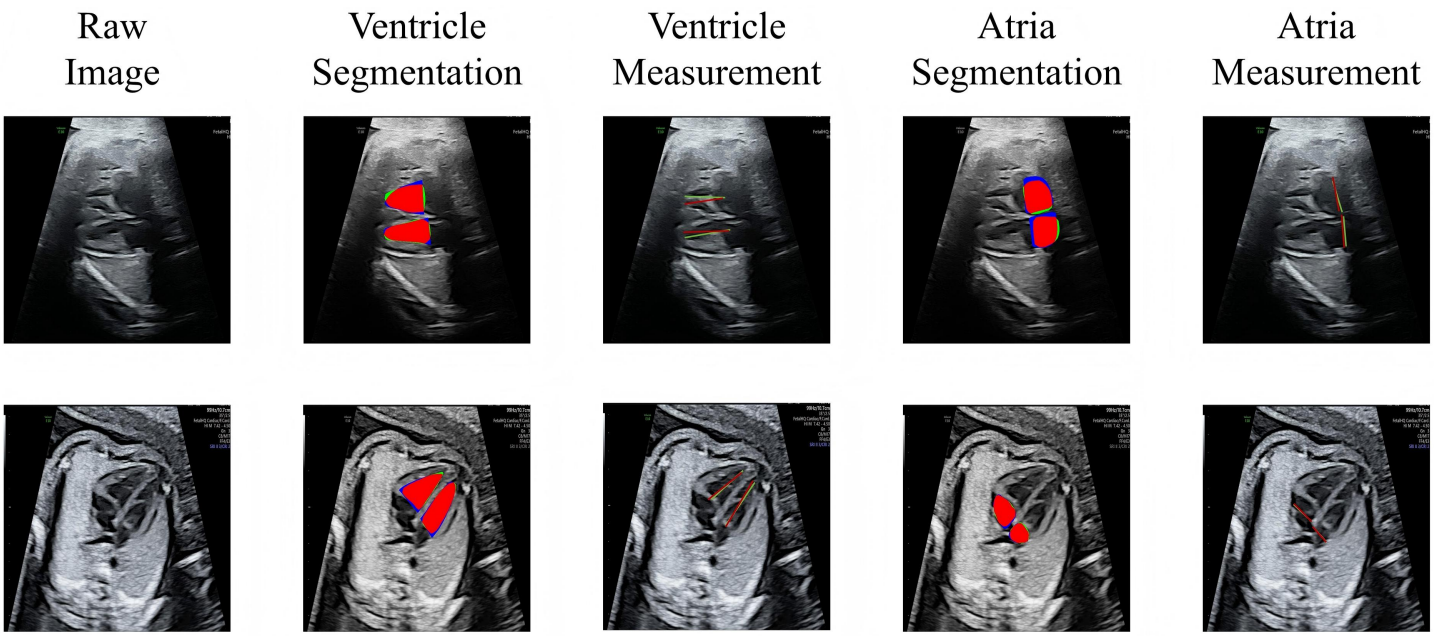

Fig. S3: Schematic diagram of video frame segmentation and measurement results for two echocardiograms. The red/green/blue regions represent correct/over-segmented/under-segmented results, respectively. The red/green straight lines indicate measurement results extracted from manual/predicted masks, respectively.

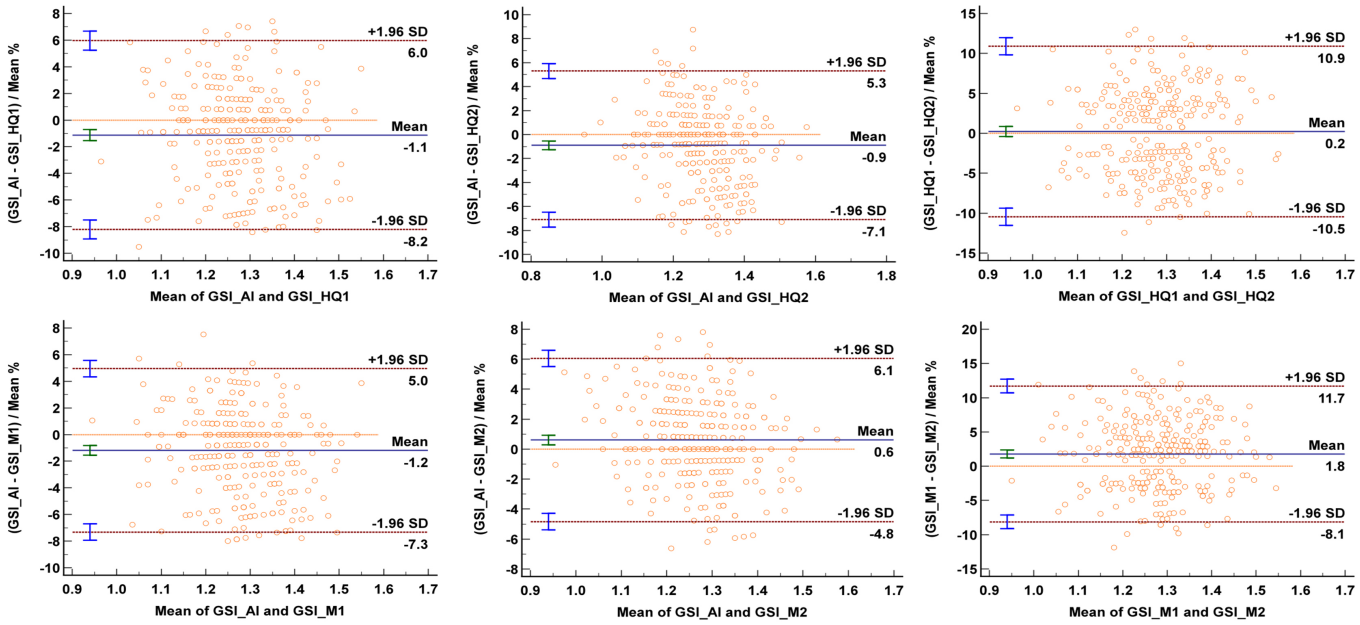

Fig. S4: The Limits of Agreement from Bland-Altman testing of Global Sphericity Index in Internal Normal Dataset

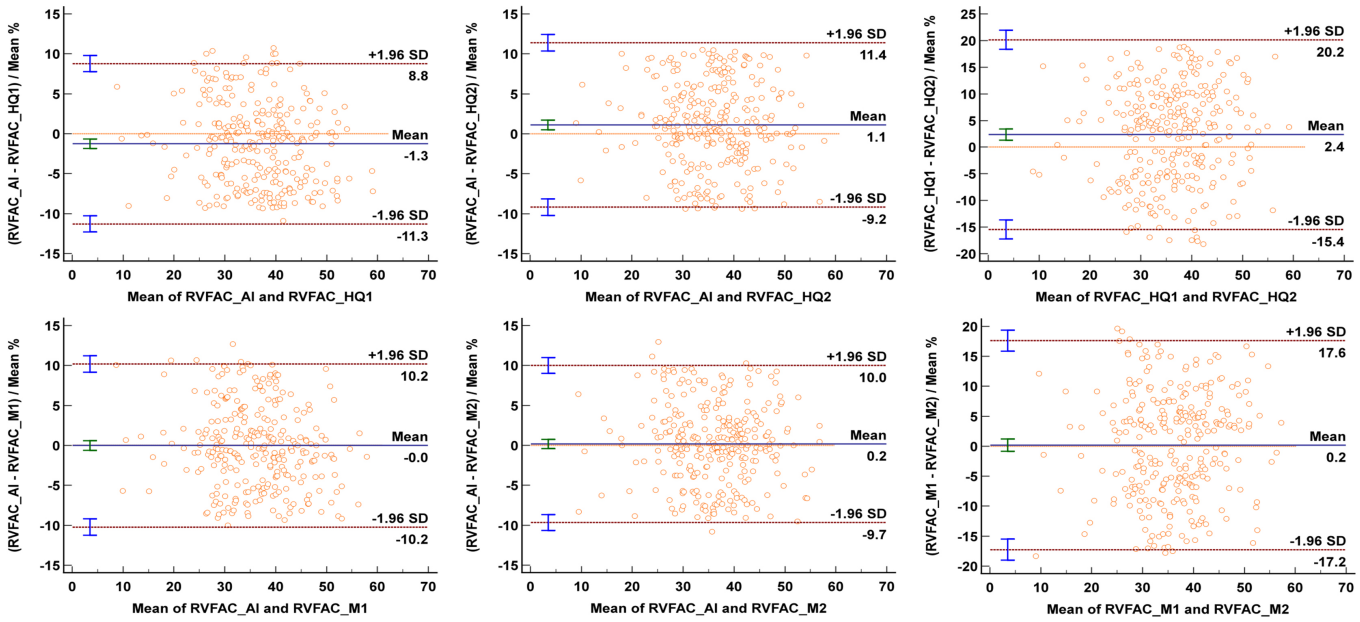

Fig. S5: The Limits of Agreement from Bland-Altman testing of Fractional Area Change of Right Ventricle in Internal Normal Dataset

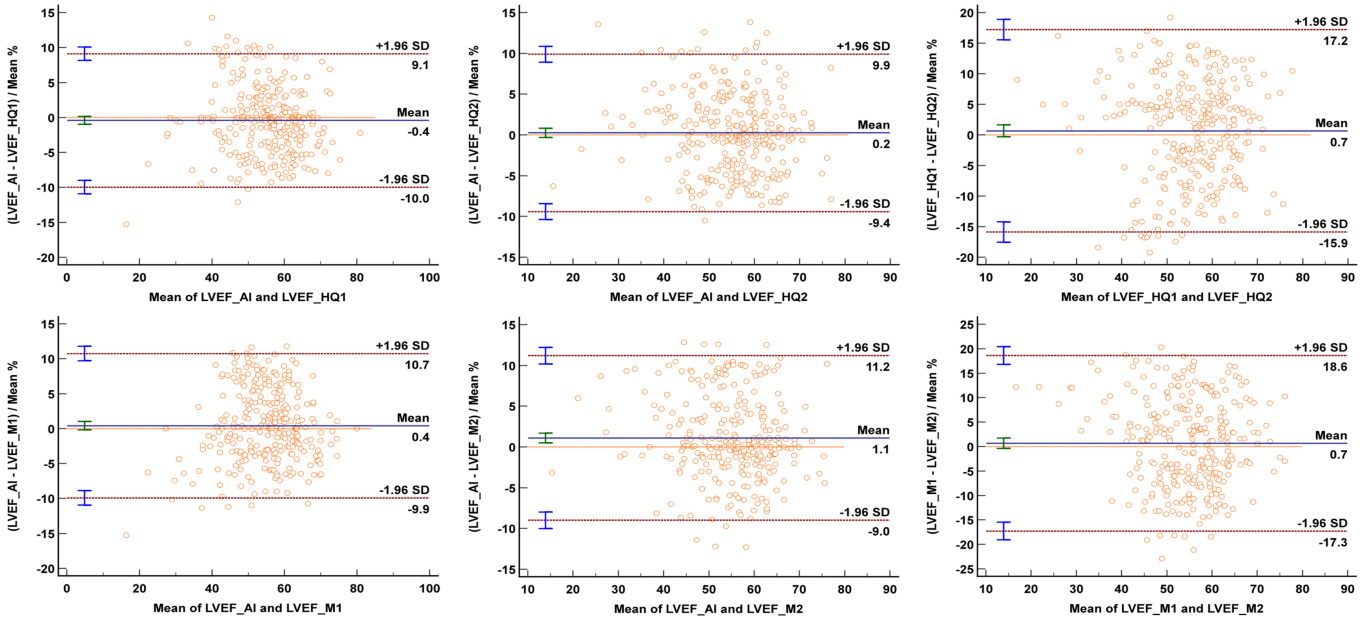

Fig. S6: The Limits of Agreement from Bland-Altman testing of Ejection Fraction of Left Ventricle in Internal Normal Dataset

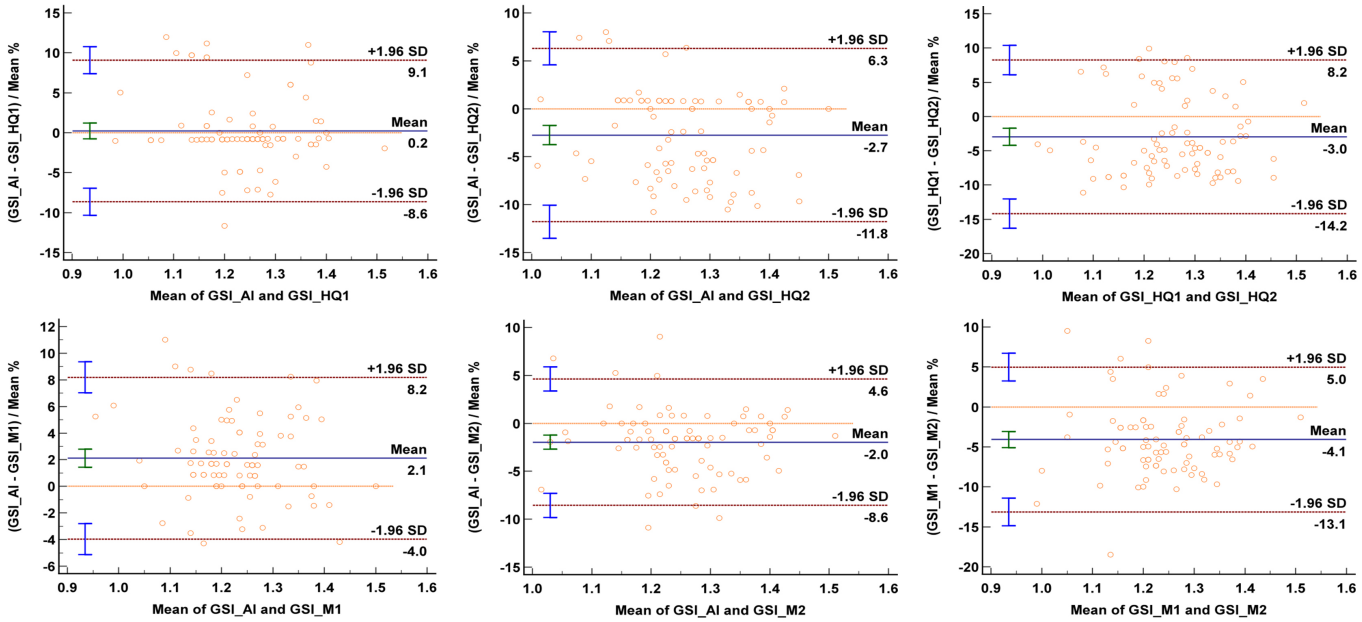

Fig. S7: The Limits of Agreement from Bland-Altman testing of Global Sphericity Index in Internal Abnormal Dataset

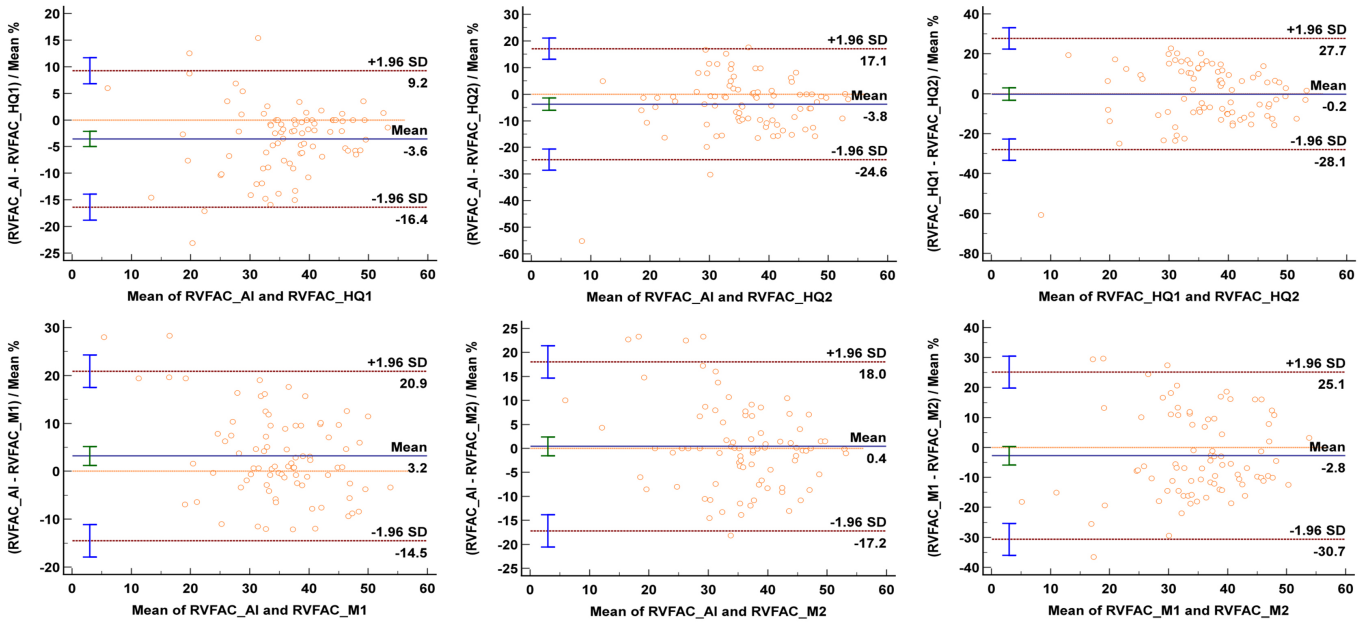

Fig. S8: The Limits of Agreement from Bland-Altman testing of Fractional Area Change of Right Ventricle in Internal Abnormal Dataset

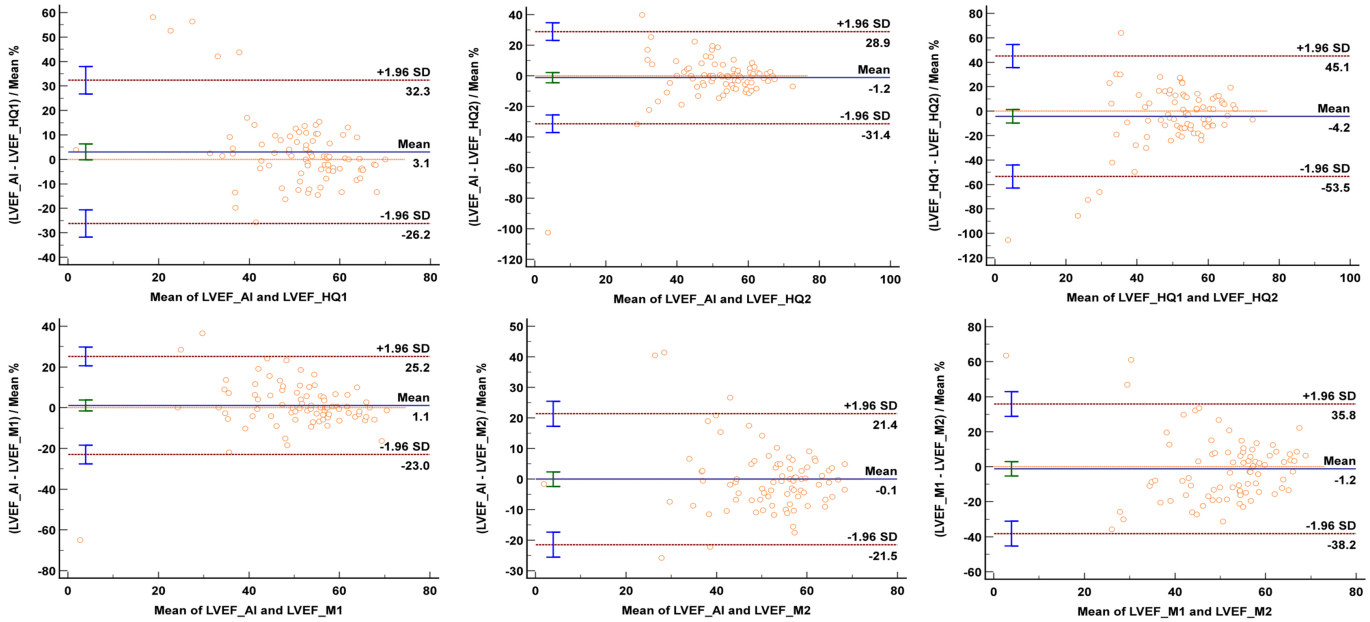

Fig. S9: The Limits of Agreement from Bland-Altman testing of Ejection Fraction of Left Ventricle in Internal Abnormal Dataset

Table S1: Training Hyperparameters and testing device of the AI Model

Hyperparameter	Value	Testing Device	Product name
epoch	200	CPU	Intel Core i7-12700
base learning rate	0.0001	GPU	Nvidia RTX 4070
warmup	true	RAM	16G
warmup steps	2000	Operator System	Window 11
clip grad by norm	0.1		
regularizer	false		
optimizer	AdamW		
weight decay	0.0001		
use focal loss	true		

Table S2: Cardiac parameters obtainable by automatic, manual, and HQ measurement for full heart structures.

	Parameter Name	Abbreviation	Heart		
			AI	HQ	Human
Routine Cardiac Parameters	Heart Rate	HR	✓	✓	✓
	Cardiac Axis	CA	✓		✓
	Cardiothoracic Area Ratio	CTAR	✓		✓
	Global Sphericity Index	GSI	✓	✓	✓
	End-diastolic Ventricular Area Ratio	EDVAR	✓	✓	✓
Expand Cardiac parameters	Cardiothoracic Ratio	CTR	✓		✓
	Cardiothoracic Circumference Ratio	CTCR	✓		✓
	End-diastolic Ventricular Width Ratio	EDVWR	✓	✓	✓
	End-diastolic Ventricular Length Ratio	EDVLR	✓	✓	✓
Basic Cardiac parameters	Cardiac Length	CL	✓	✓	✓
	Cardiac Width	CW	✓	✓	✓
	Thoracic Width	TW	✓		✓
	Cardiac Circumference	CC	✓		✓
	Thoracic Circumference	TC	✓		✓
	Cardiac Area	-	✓	✓	✓
	Thoracic Area	TA	✓		✓
	Interventricular Septum Thickness	IVST	✓		✓

Table S3: Cardiac parameters obtainable by automatic, manual, and HQ measurement for left and right heart structures. Ed and Es denotes End-diastolic and End-systolic.

	Parameter Name	Abbreviation	Left Heart			Right Heart		
			AI	HQ	Human	AI	HQ	Human
Routine Cardiac Parameters	Atrial Area	LAA, RAA	✓		✓	✓		✓
	Fractional Area Change	LVFAC, RVFAC	✓	✓	✓	✓	✓	✓
	Stroke Volume	LVSV	✓	✓	✓			
	Ejection Fraction	LVEF	✓	✓	✓			
	Cardiac Output	LVCO	✓	✓	✓			
	Ed Transverse Width	LVTWd, RVTWd	✓	✓	✓	✓	✓	✓
Expand Cardiac parameters	Annular Ventricular Fractional Shortening	LVAVFS, RVAVFS	✓	✓	✓	✓	✓	✓
	Transverse fractional shortening	LVTFS, RVTFS	✓	✓	✓	✓	✓	✓
	Sphericity Index	LVSI, RVSI	✓	✓	✓	✓	✓	✓
	Global Longitudinal Strain	LVGLS, RVGLS	✓	✓	✓	✓	✓	✓
	Septal Wall Strain	LVSWS, RVSWS	✓		✓	✓		✓
	Free Wall Strain	LVFWS, RVFWS	✓		✓	✓		✓
	Annular Plane Systolic Excursion	LVAPSE, RVAPSE	✓		✓	✓		✓
Basic Cardiac parameters	Superior-inferior Diameter	LASID, RASID	✓		✓	✓		✓
	Transverse Diameter	LATD, RATD	✓		✓	✓		✓
	Es Transverse Width	LVTWs, RVTWs	✓		✓	✓		✓
	Ed Basal-apical Length	LVBALd, RVBALd	✓	✓	✓	✓	✓	✓
	Es Basal-apical Length	LVBALs, RVBALs	✓	✓	✓	✓	✓	✓
	Ed Area	LVEAd, RVEAd	✓	✓	✓	✓	✓	✓
	Es Area	LVEAs, RVEAs	✓	✓	✓	✓	✓	✓
	Ed Endocardial Length	LVECLd, RVECLd	✓		✓	✓		✓
	Es Endocardial Length	LVECLs, RVECLs	✓		✓	✓		✓
	Ed Endocardial Septal Wall Length	LVECSWLd, RVECSWLd	✓		✓	✓		✓
	Es Endocardial Septal Wall Length	LVECSWLs, RVECSWLs	✓		✓	✓		✓
	Ed Endocardial Free Wall Length	LVECFWLd, RVECFWLd	✓		✓	✓		✓
	Es Endocardial Free Wall Length	LVECFWLs, RVECFWLs	✓		✓	✓		✓
	Es Free Wall hickness	LVFWd, RVFWd	✓		✓	✓		✓
	Ed Volume	LVEVd	✓	✓	✓			
	Es Volume	LVEVs	✓	✓	✓			

Table S4: Segmentation Performence of Six Key Cardiac Structures on Five State-of-art Methods and Our Model.

Model	Left Atrium				Right Atrium				R-Left Ventricle			
	Dice	IoU	HD	p-values	Dice	IoU	HD	p-values	Dice	IoU	HD	p-values
MaskRCNN	85.08±9.45	75.06±12.67	1,68±1.03	<0.01	88.93±6.18	80.57±9.29	1.38±0.75	<0.01	91.43±5.43	84.63±8.34	1.68±0.98	<0.01
YoloLact	81.56±12.87	73.48±14.34	2.08±0.86	<0.01	84.97±15.13	75.79±17.21	2.54±1.14	<0.01	87.33±15.77	78.70±17.94	2.44±1.13	<0.01
Mask2Former	83.09±8.85	71.94±11.55	1.95±1.17	<0.01	87.49±6.24	78.25±9.04	1.57±0.88	<0.01	89.91±6.32	82.18±8.97	1.89±1.26	<0.01
FastInst	84.51±7.75	73.88±10.61	1.78±0.97	<0.01	87.83±6.25	78.81±9.34	1.50±0.84	<0.01	90.90±4.84	83.65±7.58	1.77±1.07	<0.01
Yolov11	81.82±8.98	70.12±11.84	2.03±1.07	<0.01	86.20±6.45	76.27±9.30	1.72±0.86	<0.01	87.97±7.60	79.25±10.65	2.45±1.66	<0.01
Ours	87.76±6.20	78.70±9.25	1.40±0.71	-	89.99±4.74	82.12±7.48	1.24±0.60	-	92.43±4.17	86.19±6.70	1.44±0.69	-
	Right Ventricle				Cardiac				Thoracic			
	Dice	IoU	HD	p-values	Dice	IoU	HD	p-values	Dice	IoU	HD	p-values
MaskRCNN	90.04±5.76	82.33±8.70	1.91±1.23	<0.01	96.39±1.74	93.09±3.14	1.52±0.80	<0.01	95.45±3.95	91.49±5.55	4.41±3.15	<0.01
YoloLact	84.38±14.55	78.53±16.46	2.69±1.11	<0.01	93.35±4.69	89.72±6.78	3.69±1.02	<0.01	88.92±8.35	85.42±8.95	7.49±2.18	<0.01
Mask2Former	88.66±6.75	80.20±9.50	2.12±1.37	<0.01	95.52±3.27	91.57±4.80	1.88±1.46	<0.01	95.18±2.56	90.92±4.45	4.70±2.87	<0.01
FastInst	88.71±7.20	80.34±9.81	2.14±1.51	<0.01	95.22±3.06	91.02±4.85	1.84±1.31	<0.01	95.36±2.11	91.21±3.76	4.35±2.28	<0.01
Yolov11	86.55±8.91	77.20±11.73	2.61±1.76	<0.01	94.69±3.20	90.08±5.31	2.13±1.50	<0.01	95.43±1.97	91.32±3.53	4.31±2.20	<0.01
Ours	91.28±4.20	84.23±6.81	1.60±0.84	-	96.90±1.47	94.02±2.66	1.34±1.14	-	96.59±2.22	93.50±4.05	3.54±2.63	-

Table S5: Consistency Analysis of All Cardiac Parameters Between Automatic and Manual Measurement (M1, M2) in Normal Dataset

Function	ICC			LOA			R-value			MAE		
Parameter	AI-M1	AI-M2	M1-M2	AI-M1	AI-M2	M1-M2	AI-M1	AI-M2	M1-M2	AI-M1	AI-M2	M1-M2
Heart Parameters												
HR	0.911	0.915	0.783	0.00±0.07	0.00±0.03	0.00±0.11	0.898	0.897	0.744	3.823	3.680	7.090
CA	0.964	0.977	0.931	0.04±0.14	-0.01±0.09	-0.05±0.20	0.976	0.977	0.944	1.757	1.383	2.849
CTAR	0.817	0.891	0.647	0.04±0.10	0.01±0.05	-0.03±0.20	0.850	0.897	0.642	0.014	0.009	0.022
GSI	0.908	0.935	0.787	-0.01±0.06	0.01±0.03	0.02±0.10	0.900	0.923	0.762	0.031	0.027	0.056
EDVAR	0.924	0.949	0.848	-0.01±0.14	-0.01±0.06	0.00±0.20	0.929	0.952	0.848	0.048	0.039	0.078
CTR	0.863	0.902	0.700	0.01±0.08	0.00±0.04	-0.02±0.14	0.872	0.898	0.701	0.017	0.014	0.030
CTCR	0.785	0.869	0.650	0.02±0.05	0.00±0.03	-0.02±0.08	0.858	0.872	0.707	0.015	0.010	0.024
EDVWR	0.871	0.908	0.707	-0.02±0.14	0.02±0.06	0.04±0.22	0.885	0.915	0.730	0.064	0.053	0.111
EDVLR	0.850	0.836	0.622	0.00±0.08	0.01±0.05	0.00±0.14	0.844	0.826	0.574	0.029	0.032	0.057
CL	0.980	0.984	0.951	0.02±0.06	0.00±0.04	-0.02±0.11	0.983	0.981	0.952	0.093	0.085	0.166
CW	0.978	0.981	0.936	0.03±0.07	-0.01±0.08	-0.04±0.14	0.986	0.982	0.952	0.090	0.087	0.170
TW	0.975	0.981	0.938	0.01±0.07	-0.01±0.04	-0.02±0.12	0.977	0.979	0.942	0.153	0.138	0.271
CC	0.969	0.991	0.949	0.04±0.07	-0.01±0.02	-0.05±0.09	0.982	0.992	0.973	0.366	0.193	0.535
TC	0.983	0.985	0.957	0.01±0.07	-0.01±0.03	-0.02±0.10	0.982	0.983	0.957	0.472	0.430	0.851
Cardiac Area	0.991	0.996	0.984	0.03±0.09	0.01±0.04	-0.03±0.15	0.993	0.996	0.983	0.275	0.156	0.401
TA	0.995	0.996	0.988	0.00±0.08	0.00±0.04	0.00±0.12	0.994	0.995	0.987	0.703	0.608	1.218
IVST	0.956	0.986	0.923	0.05±0.11	0.00±0.04	-0.05±0.17	0.973	0.986	0.940	0.233	0.120	0.331
Left Heart Parameters												
LAA	0.986	0.988	0.958	-0.01±0.12	-0.02±0.06	-0.01±0.22	0.989	0.990	0.965	0.048	0.044	0.089
LVFAC	0.910	0.928	0.765	0.02±0.17	0.00±0.08	-0.02±0.29	0.895	0.912	0.719	2.787	2.369	4.957
LVSV	0.986	0.987	0.959	0.01±0.19	0.03±0.10	0.02±0.35	0.988	0.988	0.964	0.041	0.039	0.077
LVEF	0.955	0.954	0.864	0.00±0.10	0.01±0.05	0.01±0.18	0.941	0.936	0.817	2.216	2.067	4.032
LVCO	0.989	0.990	0.968	0.01±0.17	0.03±0.09	0.02±0.31	0.990	0.989	0.969	5.415	5.304	10.06
LVAVFS	0.973	0.973	0.918	0.01±0.14	-0.01±0.07	-0.01±0.25	0.973	0.976	0.921	1.216	1.260	2.364
LVTFS	0.948	0.948	0.867	0.08±0.69	0.05±0.33	-0.03±0.10	0.935	0.946	0.855	1.526	1.607	2.905
LVSI	0.875	0.910	0.707	-0.02±0.14	0.02±0.06	0.04±0.22	0.882	0.904	0.712	0.138	0.112	0.240
LVGLS	0.965	0.974	0.906	-0.03±0.13	0.03±0.06	0.06±0.21	0.966	0.971	0.908	1.452	1.150	2.482
LVSWS	0.951	0.957	0.874	-0.02±0.21	0.02±0.12	0.04±0.37	0.957	0.958	0.880	1.709	1.512	3.084
LVFWS	0.940	0.947	0.840	-0.04±0.18	0.04±0.09	0.07±0.31	0.951	0.954	0.869	2.055	1.830	3.633
LVAPSE	0.974	0.978	0.922	-0.04±0.11	0.03±0.06	0.07±0.19	0.986	0.982	0.950	0.054	0.044	0.093
LASID	0.951	0.963	0.868	-0.04±0.11	0.02±0.06	0.06±0.20	0.971	0.964	0.902	0.060	0.048	0.105
LATD	0.955	0.954	0.861	0.03±0.13	-0.04±0.06	-0.07±0.21	0.964	0.966	0.893	0.055	0.059	0.109
LVTWd	0.968	0.981	0.932	0.02±0.12	-0.01±0.05	-0.02±0.18	0.969	0.981	0.934	0.408	0.312	0.671
LVTWs	0.974	0.985	0.949	0.01±0.11	-0.01±0.04	-0.02±0.16	0.975	0.986	0.952	0.321	0.250	0.532
LVBALd	0.990	0.985	0.964	0.00±0.05	0.01±0.03	0.01±0.10	0.989	0.984	0.965	0.387	0.519	0.839
LVBALs	0.992	0.987	0.973	0.00±0.06	0.01±0.04	0.02±0.10	0.991	0.987	0.973	0.325	0.446	0.718
LVEAd	0.986	0.994	0.975	0.02±0.14	0.01±0.05	-0.01±0.21	0.983	0.993	0.969	0.083	0.052	0.123
LVEAs	0.990	0.994	0.981	0.02±0.13	0.01±0.06	0.00±0.19	0.990	0.993	0.979	0.041	0.034	0.067
LVECLd	0.991	0.972	0.948	0.01±0.05	-0.04±0.03	-0.05±0.08	0.992	0.989	0.978	0.081	0.159	0.231
LVECLs	0.985	0.972	0.933	0.03±0.06	-0.05±0.03	-0.07±0.10	0.991	0.992	0.977	0.100	0.147	0.240
LVECSWLd	0.982	0.952	0.915	0.02±0.07	-0.05±0.04	-0.07±0.11	0.983	0.978	0.962	0.055	0.096	0.140
LVECSWLs	0.979	0.959	0.912	0.03±0.09	-0.05±0.05	-0.08±0.14	0.983	0.979	0.958	0.059	0.084	0.135
LVECFWLd	0.983	0.973	0.940	0.01±0.07	-0.03±0.04	-0.04±0.12	0.981	0.981	0.953	0.064	0.084	0.141
LVECFWLs	0.973	0.969	0.912	0.03±0.10	-0.04±0.05	-0.07±0.16	0.978	0.983	0.949	0.074	0.086	0.152
LVFWd	0.967	0.955	0.886	0.01±0.11	-0.02±0.06	-0.03±0.20	0.970	0.961	0.897	0.113	0.148	0.252
LVEVd	0.995	0.996	0.988	0.01±0.13	0.02±0.07	0.01±0.22	0.995	0.995	0.987	0.047	0.043	0.083
LVEVs	0.995	0.997	0.991	0.01±0.14	0.01±0.07	0.00±0.22	0.995	0.995	0.989	0.023	0.017	0.037
Right Heart Parameters												
RAA	0.995	0.991	0.979	0.01±0.08	-0.05±0.04	-0.06±0.15	0.996	0.995	0.986	0.029	0.047	0.073
RVFAC	0.975	0.977	0.929	0.00±0.10	0.00±0.05	0.00±-0.17	0.976	0.977	0.930	1.450	1.369	2.611
RVAVFS	0.965	0.963	0.891	0.00±0.14	0.01±0.07	0.01±0.24	0.965	0.964	0.891	1.333	1.412	2.567
RVTFS	0.921	0.924	0.810	-0.13±1.21	-0.14±0.55	0.00±1.40	0.907	0.905	0.764	2.260	2.154	4.164
RVSI	0.931	0.936	0.813	0.00±0.10	0.01±0.05	0.00±0.18	0.921	0.933	0.793	0.081	0.082	0.154
RVGLS	0.969	0.971	0.909	0.00±0.12	0.00±0.06	0.00±0.21	0.970	0.971	0.909	1.080	1.074	2.032
RVSWS	0.943	0.958	0.867	-0.01±0.25	0.01±0.09	0.02±0.33	0.938	0.954	0.860	1.623	1.367	2.770
RVFWS	0.953	0.948	0.855	0.02±0.15	0.00±0.08	-0.02±0.27	0.955	0.948	0.857	1.585	1.660	3.060
RVAPSE	0.970	0.978	0.916	-0.04±0.09	0.02±0.05	0.06±0.16	0.986	0.981	0.950	0.048	0.036	0.081
RASID	0.957	0.983	0.918	-0.06±0.08	0.01±0.04	0.07±0.13	0.981	0.986	0.955	0.059	0.029	0.083
RATD	0.968	0.983	0.928	-0.06±0.07	0.02±0.04	0.08±0.12	0.990	0.987	0.971	0.056	0.032	0.084
RVTWd	0.988	0.988	0.970	0.00±0.08	0.01±0.04	0.02±0.13	0.988	0.989	0.971	0.254	0.265	0.482
RVTWs	0.989	0.987	0.972	0.00±0.09	0.02±0.04	0.01±0.13	0.989	0.988	0.973	0.244	0.268	0.466
RVBALd	0.975	0.967	0.920	0.00±0.09	0.02±0.05	0.02±0.15	0.973	0.968	0.920	0.554	0.679	1.153
RVBALs	0.985	0.980	0.950	0.00±0.08	0.02±0.04	0.02±0.14	0.982	0.980	0.950	0.411	0.486	0.837
RVEAd	0.993	0.995	0.982	0.01±0.10	0.00±0.05	-0.01±0.17	0.992	0.994	0.980	0.054	0.043	0.093
RVEAs	0.993	0.995	0.984	0.01±0.11	0.00±0.05	-0.01±0.18	0.993	0.994	0.984	0.037	0.032	0.064
RVECLd	0.990	0.980	0.961	0.00±0.05	-0.01±0.04	-0.01±0.11	0.989	0.982	0.961	0.074	0.104	0.167
RVECLs	0.990	0.982	0.961	0.00±0.07	-0.01±0.04	-0.01±0.13	0.989	0.983	0.959	0.070	0.091	0.151
RVECSWLd	0.971	0.957	0.907	0.03±0.08	-0.04±0.04	0.07±0.26	0.979	0.972	0.950	0.062	0.078	0.130
RVECSWLs	0.970	0.964	0.913	0.03±0.09	-0.04±0.05	-0.07±0.14	0.978	0.977	0.952	0.057	0.068	0.115
RVECFWLd	0.971	0.971	0.919	-0.03±0.09	0.01±0.05	0.03±0.16	0.978	0.968	0.926	0.082	0.082	0.154
RVECFWLs	0.970	0.973	0.917	-0.03±0.11	0.01±0.06	0.04±0.20	0.975	0.971	0.921	0.075	0.071	0.137
RVFWd	0.977	0.947	0.894	0.00±0.09	0.02±0.06	0.02±0.19	0.978	0.956	0.906	0.092	0.144	0.225

Table S6: Consistency Analysis of All Cardiac Parameters Between Automatic and Manual Measurement (M1, M2) in Abnormal Dataset

Function	ICC			LOA			R-value			MAE		
Parameter	AI-M1	AI-M2	M1-M2	AI-M1	AI-M2	M1-M2	AI-M1	AI-M2	M1-M2	AI-M1	AI-M2	M1-M2
Heart Parameters												
HR	0.953	0.961	0.880	0.00±0.05	-0.01±0.02	-0.01±0.08	0.952	0.964	0.876	0.920	0.857	1.663
CA	0.948	0.970	0.892	0.04±0.25	0.00±0.11	-0.04±0.40	0.952	0.972	0.899	0.981	0.798	1.580
CTAR	0.941	0.912	0.808	-0.01±0.10	0.02±0.06	0.04±0.17	0.908	0.835	0.693	0.003	0.004	0.007
GSI	0.900	0.889	0.761	0.02±0.06	-0.02±0.03	-0.04±0.09	0.927	0.895	0.840	0.010	0.010	0.018
EDVAR	0.949	0.960	0.876	-0.04±0.17	0.00±0.08	0.04±0.30	0.933	0.964	0.841	0.024	0.020	0.040
CTR	0.955	0.808	0.725	0.00±0.06	-0.01±0.06	-0.01±0.16	0.943	0.769	0.646	0.003	0.008	0.010
CTCR	0.868	0.871	0.777	0.00±0.08	-0.01±0.03	-0.02±0.10	0.827	0.812	0.682	0.004	0.004	0.007
EDVWR	0.897	0.903	0.687	-0.03±0.17	0.02±0.09	0.04±0.31	0.915	0.905	0.699	0.037	0.032	0.066
EDVLR	0.911	0.909	0.762	0.00±0.08	0.01±0.04	0.01±0.13	0.878	0.859	0.657	0.013	0.011	0.023
CL	0.987	0.983	0.960	0.00±0.07	0.00±-0.04	0.00±0.12	0.984	0.978	0.945	0.025	0.034	0.052
CW	0.978	0.975	0.926	-0.02±0.08	0.02±0.10	0.04±0.16	0.985	0.978	0.940	0.027	0.030	0.054
TW	0.973	0.924	0.854	-0.03±0.06	0.03±0.07	0.05±0.19	0.985	0.934	0.886	0.047	0.097	0.133
CC	0.987	0.985	0.968	0.01±0.06	-0.01±0.03	-0.02±0.10	0.985	0.984	0.965	0.083	0.081	0.149
TC	0.991	0.988	0.971	0.01±0.05	0.01±0.03	0.00±0.09	0.984	0.981	0.953	0.120	0.159	0.261
Cardiac Area	0.993	0.985	0.970	-0.01±0.09	0.02±0.07	0.03±0.20	0.992	0.982	0.966	0.076	0.106	0.169
TA	0.993	0.996	0.984	0.00±0.08	0.00±0.04	-0.01±0.13	0.990	0.992	0.977	0.241	0.197	0.397
IVST	0.955	0.961	0.877	0.03±0.15	0.00±0.07	-0.02±0.26	0.959	0.964	0.885	0.077	0.071	0.137
Left Heart Parameters												
LAA	0.977	0.981	0.927	-0.01±0.14	0.00±0.07	0.01±0.26	0.987	0.985	0.958	0.016	0.015	0.029
LVFAC	0.929	0.912	0.785	0.00±0.26	-0.02±0.17	-0.02±0.36	0.892	0.904	0.723	0.816	0.856	1.522
LVSV	0.968	0.975	0.909	0.01±0.33	-0.01±0.16	-0.03±0.54	0.981	0.977	0.941	0.017	0.016	0.032
LVEF	0.928	0.925	0.796	0.01±0.24	0.00±0.11	-0.01±0.37	0.906	0.897	0.729	0.921	0.956	1.792
LVCO	0.966	0.976	0.907	0.01±0.33	-0.02±0.16	-0.04±0.55	0.980	0.979	0.942	2.513	2.413	4.760
LVAVFS	0.941	0.966	0.888	-0.05±0.18	0.01±0.08	0.06±0.26	0.954	0.967	0.903	0.491	0.447	0.851
LVTFS	0.944	0.947	0.880	-0.20±1.22	-0.10±0.77	0.06±1.48	0.936	0.952	0.873	0.801	0.800	1.468
LVSI	0.947	0.922	0.797	-0.01±0.10	0.01±0.06	0.02±0.20	0.938	0.927	0.790	0.061	0.054	0.114
LVGLS	0.944	0.948	0.866	-0.04±0.19	-0.03±0.11	0.01±0.35	0.959	0.950	0.870	0.559	0.554	1.014
LVSWS	0.873	0.875	0.760	-0.01±0.38	-0.03±0.25	-0.02±0.67	0.833	0.879	0.684	0.707	0.759	1.321
LVFWS	0.891	0.869	0.771	-0.05±0.20	-0.01±0.12	0.03±0.36	0.947	0.928	0.833	0.680	0.749	1.268
LVAPSE	0.980	0.979	0.939	0.01±0.14	0.02±0.07	0.01±0.24	0.980	0.981	0.940	0.013	0.014	0.025
LASID	0.966	0.957	0.882	0.00±0.13	0.02±0.08	0.02±0.24	0.965	0.959	0.884	0.014	0.018	0.030
LATD	0.940	0.915	0.799	-0.01±0.15	0.03±0.08	0.04±0.27	0.947	0.922	0.813	0.016	0.019	0.033
LVTWd	0.983	0.974	0.935	0.01±0.10	-0.01±0.06	-0.02±0.19	0.983	0.975	0.936	0.092	0.110	0.193
LVTWs	0.970	0.965	0.896	0.01±0.11	0.00±0.06	-0.02±0.22	0.966	0.960	0.884	0.115	0.115	0.221
LVBALd	0.980	0.978	0.952	-0.01±0.07	0.00±0.04	0.01±0.12	0.974	0.974	0.939	0.203	0.191	0.357
LVBALs	0.987	0.990	0.971	0.00±0.07	0.00±0.03	-0.01±0.10	0.976	0.981	0.947	0.104	0.080	0.170
LVEAd	0.979	0.979	0.931	0.02±0.16	-0.02±0.07	-0.04±0.27	0.979	0.984	0.951	0.049	0.047	0.093
LVEAs	0.981	0.982	0.941	0.02±0.15	0.01±0.08	-0.03±0.25	0.982	0.983	0.943	0.015	0.013	0.028
LVECLd	0.991	0.992	0.974	-0.01±0.05	-0.01±0.02	0.00±0.09	0.991	0.993	0.975	0.024	0.024	0.043
LVECLs	0.988	0.992	0.970	0.01±0.06	0.00±0.03	-0.01±0.10	0.984	0.986	0.958	0.020	0.018	0.036
LVECSWLd	0.976	0.979	0.944	0.00±0.08	-0.01±0.04	-0.01±0.13	0.979	0.985	0.951	0.016	0.015	0.028
LVECSWLs	0.978	0.984	0.946	0.01±0.08	0.00±0.04	-0.01±0.13	0.979	0.985	0.948	0.014	0.011	0.023
LVECFWLd	0.984	0.982	0.961	-0.01±0.08	0.00±0.04	0.01±0.13	0.975	0.977	0.933	0.018	0.019	0.032
LVECFWLs	0.978	0.984	0.944	0.01±0.09	0.00±0.04	-0.01±0.15	0.963	0.972	0.914	0.017	0.014	0.029
LVFWd	0.992	0.994	0.983	-0.01±0.11	0.00±0.05	0.02±0.16	0.971	0.979	0.937	0.030	0.026	0.053
LVEVd	0.990	0.993	0.974	0.00±0.13	-0.01±0.06	-0.01±0.23	0.991	0.995	0.980	0.017	0.016	0.031
LVEVs	0.993	0.992	0.979	-0.01±0.14	0.00±0.06	0.00±0.21	0.995	0.995	0.988	0.007	0.007	0.012
Right Heart Parameters												
RAA	0.987	0.988	0.964	0.02±0.13	0.00±0.07	-0.02±0.22	0.985	0.985	0.962	0.016	0.016	0.029
RVFAC	0.950	0.954	0.885	0.03±0.18	0.00±0.09	-0.03±0.28	0.955	0.956	0.887	0.635	0.588	1.128
RVAVFS	0.935	0.904	0.797	-0.02±0.40	0.02±0.13	0.04±0.50	0.938	0.906	0.798	0.495	0.632	1.026
RVTFS	0.924	0.916	0.800	-0.10±1.06	-0.13±0.56	-0.05±1.20	0.941	0.938	0.860	1.083	1.009	1.927
RVSI	0.892	0.900	0.644	0.01±0.15	0.00±0.07	-0.01±0.28	0.897	0.901	0.643	0.033	0.031	0.062
RVGLS	0.942	0.951	0.867	-0.04±0.21	-0.01±0.09	0.03±0.34	0.949	0.958	0.868	0.451	0.396	0.788
RVSWS	0.899	0.944	0.861	-0.06±0.35	-0.04±0.13	0.02±0.43	0.912	0.953	0.861	0.705	0.475	1.002
RVFWS	0.928	0.930	0.821	-0.01±0.19	0.01±0.11	0.02±0.34	0.901	0.916	0.767	0.565	0.548	1.038
RVAPSE	0.975	0.970	0.919	-0.01±0.14	0.04±0.07	0.05±0.25	0.975	0.975	0.927	0.015	0.016	0.028
RASID	0.975	0.977	0.935	0.00±0.10	0.02±0.05	0.02±0.16	0.969	0.976	0.926	0.012	0.012	0.022
RATD	0.978	0.980	0.943	0.00±0.10	0.01±0.05	0.01±0.16	0.978	0.981	0.942	0.012	0.012	0.022
RVTWd	0.962	0.971	0.897	-0.02±0.13	0.00±0.06	0.02±0.23	0.967	0.972	0.899	0.170	0.138	0.296
RVTWs	0.979	0.979	0.936	-0.02±0.11	0.01±0.05	0.02±0.19	0.981	0.980	0.939	0.145	0.136	0.257
RVBALd	0.976	0.965	0.924	-0.01±0.08	0.01±0.05	0.01±0.16	0.977	0.967	0.925	0.185	0.224	0.371
RVBALs	0.987	0.981	0.962	0.00±0.07	0.00±0.04	0.01±0.12	0.988	0.981	0.962	0.101	0.117	0.202
RVEAd	0.994	0.996	0.988	-0.02±0.09	-0.01±0.03	0.01±0.14	0.990	0.996	0.984	0.014	0.011	0.024
RVEAs	0.993	0.995	0.987	-0.03±0.10	-0.01±0.05	0.02±0.15	0.991	0.994	0.981	0.014	0.011	0.023
RVECLd	0.993	0.993	0.980	0.00±0.05	-0.01±0.02	-0.01±0.08	0.993	0.994	0.980	0.021	0.019	0.037
RVECLs	0.991	0.996	0.981	0.01±0.05	0.00±0.02	-0.01±0.08	0.990	0.993	0.978	0.018	0.012	0.028
RVECSWLd	0.982	0.986	0.955	0.00±0.08	-0.01±0.03	-0.01±0.12	0.982	0.987	0.956	0.014	0.012	0.024
RVECSWLs	0.972	0.990	0.955	0.02±0.09	0.00±0.03	-0.02±0.12	0.976	0.990	0.957	0.015	0.008	0.020
RVECFWLd	0.987	0.988	0.963	-0.01±0.07	-0.01±0.03	0.00±0.12	0.987	0.989	0.962	0.017	0.016	0.031
RVECFWLs	0.990	0.993	0.975	0.00±0.07	-0.01±0.03	0.00±0.12	0.989	0.987	0.968	0.013	0.010	0.022
RVFWd	0.931	0.929	0.783	-0.01±0.17	0.01±0.09	0.02±0.30	0.931	0.930	0.784	0.062	0.065	0.118

Table S7: Consistency Analysis of All Cardiac Parameters Between Automatic and HQ Measurement (HQ1, HQ2) in Normal Dataset

Function	ICC			LOA			R-value			MAE		
Parameter	AI-HQ1	AI-HQ2	HQ1-HQ2	AI-HQ1	AI-HQ2	HQ1-HQ2	AI-HQ1	AI-HQ2	HQ1-HQ2	AI-HQ1	AI-HQ2	HQ1-HQ2
Heart Parameters												
HR	0.920	0.931	0.811	0.02±0.06	0.00±0.06	-0.02±0.10	0.931	0.921	0.793	3.853	3.333	6.847
GSI	0.880	0.911	0.769	-0.01±0.07	-0.01±0.06	0.00±0.11	0.869	0.910	0.733	0.036	0.031	0.060
EDVAR	0.926	0.951	0.838	0.02±0.13	0.00±0.11	-0.01±0.21	0.930	0.953	0.840	0.048	0.038	0.080
EDVWR	0.910	0.842	0.669	0.00±0.12	0.04±0.15	0.04±0.23	0.912	0.870	0.691	0.052	0.071	0.116
EDVLR	0.861	0.871	0.661	0.00±0.08	0.01±0.08	-0.01±0.13	0.847	0.866	0.617	0.027	0.027	0.052
CL	0.961	0.978	0.929	0.03±0.10	0.02±0.08	-0.01±0.16	0.966	0.981	0.922	0.128	0.095	0.205
CW	0.940	0.966	0.881	0.03±0.14	0.03±0.11	-0.01±0.22	0.952	0.970	0.882	0.142	0.102	0.232
Cardiac Area	0.985	0.993	0.967	0.04±0.11	-0.02±0.09	-0.05±0.18	0.989	0.992	0.974	0.358	0.247	0.572
Left Heart Parameters												
LVFAC	0.920	0.933	0.783	-0.01±0.17	0.00±0.14	0.00±0.27	0.913	0.918	0.750	2.652	2.235	4.685
LVSV	0.988	0.989	0.964	-0.03±0.16	0.00±0.18	0.02±0.31	0.992	0.990	0.971	0.038	0.038	0.073
LVEF	0.964	0.960	0.889	0.00±0.10	0.00±0.10	0.01±0.17	0.958	0.944	0.862	1.928	2.054	3.746
LVCO	0.992	0.992	0.972	-0.01±0.15	0.00±0.15	0.01±0.28	0.993	0.993	0.977	4.884	4.806	9.506
LVAVFS	0.977	0.972	0.923	0.02±0.15	-0.01±0.14	-0.04±0.26	0.979	0.975	0.929	1.208	1.330	2.431
LVTFS	0.977	0.977	0.942	0.03±0.76	0.04±0.94	0.01±1.27	0.968	0.970	0.930	1.311	1.336	2.369
LVSI	0.899	0.863	0.704	0.00±0.13	0.04±0.13	0.04±0.22	0.887	0.888	0.708	0.113	0.145	0.240
LVGLS	0.939	0.972	0.907	-0.06±0.17	-0.03±0.13	0.04±0.24	0.944	0.958	0.875	1.888	1.134	2.652
LVTWd	0.972	0.961	0.923	-0.01±0.11	-0.04±0.11	-0.02±0.19	0.972	0.971	0.921	0.355	0.474	0.758
LVBALd	0.989	0.991	0.971	-0.01±0.05	0.01±0.05	0.02±0.08	0.991	0.991	0.975	0.367	0.369	0.698
LVBALs	0.988	0.989	0.966	-0.02±0.06	0.01±0.07	0.03±0.11	0.996	0.991	0.974	0.400	0.431	0.799
LVEAd	0.988	0.995	0.978	-0.02±0.13	0.00±0.09	0.02±0.19	0.987	0.994	0.974	0.081	0.048	0.118
LVEAs	0.991	0.995	0.980	-0.01±0.13	0.00±0.10	0.01±0.19	0.990	0.994	0.979	0.041	0.030	0.067
LVEVd	0.996	0.996	0.989	-0.02±0.11	-0.01±0.13	0.02±0.21	0.996	0.995	0.987	0.043	0.046	0.083
LVEVs	0.995	0.996	0.988	-0.01±0.14	-0.01±0.15	0.01±0.24	0.995	0.995	0.986	0.024	0.021	0.042
Right Heart Parameters												
RVFAC	0.974	0.972	0.916	-0.01±0.10	0.01±0.10	0.02±0.18	0.976	0.973	0.922	1.515	1.503	2.822
RVAVFS	0.965	0.966	0.896	0.00±0.14	0.01±0.13	0.01±0.24	0.966	0.966	0.897	1.354	1.327	2.503
RVTFS	0.971	0.982	0.936	-0.31±0.93	-0.01±1.12	0.31±1.00	0.980	0.979	0.944	1.588	1.180	2.475
RVSI	0.945	0.924	0.805	0.00±0.09	0.01±0.11	0.01±0.18	0.939	0.914	0.781	0.072	0.087	0.152
RVGLS	0.933	0.945	0.833	0.01±0.19	-0.01±0.16	0.03±0.30	0.935	0.947	0.836	1.754	1.600	3.148
RVTWd	0.989	0.987	0.966	-0.01±0.07	0.00±0.09	0.02±0.13	0.991	0.987	0.969	0.261	0.285	0.523
RVBALd	0.978	0.973	0.927	-0.01±0.08	0.01±0.08	0.03±0.14	0.978	0.973	0.929	0.562	0.625	1.130
RVBALs	0.985	0.984	0.952	-0.01±0.08	0.01±0.08	0.02±0.14	0.984	0.984	0.954	0.432	0.451	0.846
RVEAd	0.993	0.995	0.982	-0.01±0.10	0.00±0.09	0.01±0.18	0.993	0.994	0.979	0.053	0.044	0.094
RVEAs	0.993	0.996	0.984	0.00±0.11	0.00±0.09	-0.01±0.18	0.993	0.995	0.984	0.038	0.030	0.063

Table S8: Consistency Analysis of All Cardiac Parameters Between Automatic and HQ Measurement (HQ1, HQ2) in Abnormal Dataset

Function	ICC			LOA			R-value			MAE		
Parameter	AI-HQ1	AI-HQ2	HQ1-HQ2	AI-HQ1	AI-HQ2	HQ1-HQ2	AI-HQ1	AI-HQ2	HQ1-HQ2	AI-HQ1	AI-HQ2	HQ1-HQ2
Heart Parameters												
HR	0.962	0.965	0.897	-0.01±0.05	0.01±0.05	0.01±0.08	0.957	0.965	0.898	2.988	3.012	5.687
GSI	0.857	0.800	0.740	0.00±0.09	-0.03±0.09	-0.03±0.11	0.865	0.842	0.744	0.037	0.052	0.073
EDVAR	0.956	0.953	0.868	-0.04±0.17	0.00±0.19	0.03±0.33	0.950	0.940	0.825	0.082	0.087	0.156
EDVWR	0.930	0.913	0.756	0.01±0.15	0.00±0.17	-0.01±0.29	0.929	0.922	0.763	0.072	0.092	0.157
EDVLR	0.881	0.894	0.692	0.02±0.08	0.00±0.08	-0.02±0.14	0.870	0.868	0.618	0.037	0.033	0.066
CL	0.951	0.974	0.914	-0.01±0.14	0.01±0.10	0.02±0.19	0.947	0.958	0.881	0.177	0.114	0.263
CW	0.938	0.945	0.817	-0.01±0.17	0.04±0.13	0.05±0.27	0.946	0.958	0.843	0.194	0.169	0.343
Cardiac Area	0.989	0.987	0.966	0.00±0.11	-0.01±0.13	-0.01±0.21	0.987	0.986	0.963	0.324	0.380	0.647
Left Heart Parameters												
LVFAC	0.947	0.939	0.848	0.01±0.22	-0.02±0.16	-0.03±0.30	0.926	0.910	0.791	2.313	2.526	4.491
LVSV	0.965	0.978	0.907	0.04±0.40	0.00±0.36	-0.04±0.64	0.975	0.981	0.942	0.065	0.052	0.113
LVEF	0.897	0.924	0.746	0.03±0.29	-0.01±0.30	-0.04±0.49	0.868	0.908	0.687	4.159	3.354	7.263
LVCO	0.959	0.978	0.897	0.03±0.40	0.00±0.36	-0.03±0.64	0.974	0.980	0.933	9.852	7.619	16.650
LVAVFS	0.979	0.928	0.900	-0.01±0.11	-0.03±0.25	-0.03±0.30	0.980	0.940	0.905	0.780	0.1.705	2.199
LVTFS	0.932	0.963	0.854	-0.15±1.19	-0.13±1.14	0.13±1.11	0.938	0.965	0.853	2.931	1.822	4.334
LVSI	0.909	0.910	0.715	0.01±0.14	-0.01±0.14	-0.02±0.25	0.906	0.917	0.724	0.136	0.148	0.270
LVGLS	0.904	0.902	0.835	-0.03±0.23	-0.04±0.26	-0.01±0.33	0.911	0.914	0.834	2.036	2.107	3.482
LVTWd	0.965	0.967	0.885	-0.01±0.13	0.01±0.13	0.02±0.25	0.966	0.968	0.885	0.466	0.469	0.911
LVBALd	0.983	0.972	0.946	0.00±0.07	-0.01±0.09	0.00±0.13	0.988	0.943	0.927	0.506	0.661	1.061
LVBALs	0.985	0.982	0.960	0.00±0.07	0.01±0.08	0.00±0.11	0.985	0.961	0.945	0.388	0.341	0.676
LVEAd	0.980	0.977	0.929	0.02±0.15	-0.03±0.15	-0.04±0.27	0.981	0.985	0.951	0.097	0.104	0.194
LVEAs	0.987	0.986	0.960	0.01±0.12	-0.01±0.12	-0.03±0.21	0.987	0.987	0.962	0.041	0.043	0.082
LVEVd	0.990	0.992	0.970	0.01±0.14	0.01±0.12	0.00±0.23	0.993	0.995	0.984	0.064	0.050	0.107
LVEVs	0.990	0.993	0.975	0.00±0.15	0.01±0.13	0.01±0.23	0.994	0.994	0.985	0.029	0.025	0.051
Right Heart Parameters												
RVFAC	0.967	0.930	0.889	-0.04±0.13	-0.04±0.21	0.00±0.28	0.976	0.939	0.889	1.731	2.668	3.912
RVAVFS	0.903	0.891	0.734	0.03±0.44	-0.03±0.34	-0.05±0.55	0.910	0.912	0.762	2.134	2.500	4.432
RVTFS	0.959	0.972	0.911	-0.11±1.08	-0.08±0.91	0.04±1.05	0.959	0.973	0.908	2.129	1.730	3.550
RVSI	0.901	0.894	0.692	0.02±0.13	-0.01±0.14	-0.03±0.25	0.909	0.905	0.707	0.107	0.111	0.208
RVGLS	0.916	0.883	0.740	-0.01±0.22	0.03±0.26	0.03±0.40	0.917	0.891	0.742	2.146	2.733	4.372
RVTWd	0.982	0.974	0.937	0.00±0.09	0.01±0.13	0.01±0.18	0.981	0.976	0.939	0.375	0.516	0.842
RVBALd	0.968	0.959	0.909	0.02±0.10	-0.01±0.11	-0.03±0.17	0.972	0.963	0.915	0.789	0.905	1.525
RVBALs	0.985	0.983	0.959	0.01±0.07	0.01±0.08	0.00±0.12	0.986	0.983	0.959	0.417	0.405	0.759
RVEAd	0.995	0.985	0.979	-0.01±0.09	-0.02±0.12	-0.01±0.17	0.992	0.991	0.978	0.045	0.073	0.111
RVEAs	0.995	0.994	0.985	0.01±0.08	0.00±0.10	-0.01±0.15	0.995	0.994	0.986	0.034	0.042	0.071

Table S9: Regression equation of mean value for the candidate.

Linear Polynomial	Fractional Polynomial		
$Y = \beta_0 + \beta_1/X^2$	$Y = \beta_0 + \beta_1/X^2 + \beta_2 \times LN(X)/X^2$	$Y = \beta_0 + \beta_1/X^2 + \beta_2/X$	$Y = \beta_0 + \beta_1/X^2 + \beta_2/X^{0.5}$
$Y = \beta_0 + \beta_1/X$	$Y = \beta_0 + \beta_1/X^2 + \beta_2 \times LN(X)$	$Y = \beta_0 + \beta_1/X^2 + \beta_2 \times X^{0.5}$	$Y = \beta_0 + \beta_1/X^2 + \beta_2 \times X$
$Y = \beta_0 + \beta_1/X^{0.5}$	$Y = \beta_0 + \beta_1/X^2 + \beta_2 \times X^2$	$Y = \beta_0 + \beta_1/X^2 + \beta_2 \times X^3$	$Y = \beta_0 + \beta_1/X + \beta_2 \times LN(X)/X$
$Y = \beta_0 + \beta_1 \times LN(X)$	$Y = \beta_0 + \beta_1/X + \beta_2/X^{0.5}$	$Y = \beta_0 + \beta_1/X + \beta_2 \times LN(X)$	$Y = \beta_0 + \beta_1/X + \beta_2 \times X^{0.5}$
$Y = \beta_0 + \beta_1 \times X^{0.5}$	$Y = \beta_0 + \beta_1/X + \beta_2 \times X$	$Y = \beta_0 + \beta_1/X + \beta_2 \times X^2$	$Y = \beta_0 + \beta_1/X + \beta_2 \times X^3$
$Y = \beta_0 + \beta_1 \times X$	$Y = \beta_0 + \beta_1/X^{0.5} + \beta_2 \times LN(X)/X^{0.5}$	$Y = \beta_0 + \beta_1/X^{0.5} + \beta_2 \times LN(X)$	$Y = \beta_0 + \beta_1/X^{0.5} + \beta_2 \times X^{0.5}$
$Y = \beta_0 + \beta_1 \times X^2$	$Y = \beta_0 + \beta_1/X^{0.5} + \beta_2 \times X$	$Y = \beta_0 + \beta_1/X^{0.5} + \beta_2 \times X^2$	$Y = \beta_0 + \beta_1/X^{0.5} + \beta_2 \times X^3$
$Y = \beta_0 + \beta_1 \times X^3$	$Y = \beta_0 + \beta_1 \times LN(X) + \beta_2 \times LN(X) \times LN(X)$	$Y = \beta_0 + \beta_1 \times LN(X) + \beta_2 \times X^{0.5}$	$Y = \beta_0 + \beta_1 \times LN(X) + \beta_2 \times X$
	$Y = \beta_0 + \beta_1 \times LN(X) + \beta_2 \times X^2$	$Y = \beta_0 + \beta_1 \times LN(X) + \beta_2 \times X^3$	$Y = \beta_0 + \beta_1 \times X^{0.5} + \beta_2 \times LN(X) \times X^{0.5}$
	$Y = \beta_0 + \beta_1 \times X^{0.5} + \beta_2 \times X$	$Y = \beta_0 + \beta_1 \times X^{0.5} + \beta_2 \times X^2$	$Y = \beta_0 + \beta_1 \times X^{0.5} + \beta_2 \times X^3$
	$Y = \beta_0 + \beta_1 \times X + \beta_2 \times LN(X) \times X$	$Y = \beta_0 + \beta_1 \times X + \beta_2 \times X^2$	$Y = \beta_0 + \beta_1 \times X + \beta_2 \times X^3$
	$Y = \beta_0 + \beta_1 \times X^2 + \beta_2 \times LN(X) \times X^2$	$Y = \beta_0 + \beta_1 \times X^2 + \beta_2 \times X^3$	$Y = \beta_0 + \beta_1 \times X^2 + \beta_2 \times LN(X) \times X^3$

Table S10: Regression function of the Z-score modeling for cardiac parameters of full heart structures. $1st$ and $2nd$ formulation are the two with the highest correlation coefficients R^2.

Function	$1st$ Formulation			$2nd$ Formulation		
Parameter	Mean	SD	R^2	Mean	SD	R^2
HR	149.6629-3.689064E-06$\times EFW^2$+ 1.056245E-09$\times EFW^3$	8.841021+ 0.001618028$\times EFW$	0.034759	127.6428-7171147$/HC^2$+ 1516022$\times LN(HC)/HC^2$	4.919184+ 0.02320865$\times HC$	0.034328
CA	40.07232-0.02836264$\times FL^2$+ 0.006222869$\times LN(FL) \times FL^2$	5.399282+ 0.04821111$\times FL$	0.021426	130.057+3.328097$\times LMP_GA$- 36.54348$\sqrt{LMP_GA}$	5.176043+ 0.1037263$\times LMP_GA$	0.019778
CTR	0.06943181+0.03436656$\times FL$- 0.006609934$\times LN(FL) \times FL$	0.03619763+ 1.892757E-05$\times FL$	0.280388	0.4899465+3.360527$/LMP_GA$- 88.60789$/LMP_GA^2$	0.03485409+ 9.081618E-05$\times LMP_GA$	0.280225
CTCR	0.4361377-10.47493$/LMP_GA$+ 3.84387$\times LN(LMP_GA)/LMP_GA$	0.02788558- 6.343736E-05$\times LMP_GA$	0.170298	0.528316+26583.53$/EFW^2$- 5392.992$\times LN(EFW)/EFW^2$	0.02665586- 3.990839E-07$\times EFW$	0.169187
CTAR	0.3040152-36.41152$/LMP_GA^2$+ 2.205871$\times LN(LMP_GA)/LMP_GA^2$	0.02465275+ 0.0001211303$\times LMP_GA$	0.222895	0.03457541+0.01753121$\times FL$- 0.003302323$\times LN(FL)/FL$	0.02610358+ 3.581381E-05$\times FL$	0.219855
GSI	-0.5568765+0.09644219$\times\sqrt{BPD}$+ 8.408515$/\sqrt{BPD}$	0.0991837- 0.0002080715$\times BPD$	0.093694	1.236462-44314.04$/EFW^2$- 9469.965$\times LN(EFW)/EFW^2$	0.08786284- 2.384998E-06$\times EFW$	0.091471
CL	-3.356458+0.9641188$\times LN(EFW)$+ 3.249074E-08$\times EFW^2$	0.1313604+ 5.910062E-05$\times EFW$	0.906223	-6.955881+3.070029$\times LN(US_MGA)$+ 1.077453E-05$\times US_MGA^3$	-0.01692692+ 0.008408916$\times US_MGA$	0.897296
CW	-3.306363+0.8593715$\times LN(EFW)$+ 1.767769E-08$\times EFW^2$	0.09234226+ 5.938688E-05$\times EFW$	0.916652	-6.842721+2.85534$\times LN(US_MGA)$+ 5.733709E-06$\times US_MGA^3$	-0.05760828+ 0.008496058$\times US_MGA$	0.907767
TW	-8.941337+1.925492$\times LN(EFW)$+ 27.66845$/\sqrt{EFW}$	0.1852984+ 0.000134212$\times EFW$	0.833449	15.81322+5232.405$/AC$- 1406.252$\times LN(AC)/AC$	-0.07518709+ 0.00183677$\times AC$	0.830096
CC	-11.40034+3.126136$\times LN(EFW)$+ 8.910363E-08$\times EFW^2$	0.3079648+ 0.0001739626$\times EFW$	0.939464	-23.4788+10.10333/ $\times LN(US\_MGA)$+ 2.975808E-05$\times US_MGA^3$	-0.09647272+ 0.02393333$\times US_MGA$	0.93025
TC	-21.95691+6.009783$\times LN(EFW)$+ 66511.52$/EFW^2$	0.3662421+ 0.0003508531$\times EFW$	0.948847	-61.07274+24.02197/ $\times LN(US\_MGA)$+ 1232.189$/US_MGA^2$	-0.3098846+ 0.04250003$\times US_MGA$	0.940487
Cardiac Area	-11.71449+0.002266213$\times EFW$+ 2.416003$\times LN(EFW)$	0.1779864+ 0.0004873562$\times EFW$	0.93456	-13.02187+3.411787$\times\sqrt{US_MGA}$+ 0.0001379828$\times US_MGA^3$	-1.06166+ 0.06892101$\times US_MGA$	0.925343
TA	-11.161+1.944155$\times\sqrt{EFW}$- 0.1095987$\times LN(EFW) \times \sqrt{EFW}$	0.315133+ 0.001727302$\times EFW$	0.935068	-19.6171+1.578279$\times US_MGA$+ 0.0001965536$\times US_MGA^3$	-3.460649+ 0.2183501$\times US_MGA$	0.928075
IVST	-3.510073+1.077596$\times LN(EFW)$+ 7.839812E-08$\times EFW^2$	0.5560803+ 0.0001536073$\times EFW$	0.499956	5.467122-58.66158$/US_MGA$+ 3.883713E-05$\times US_MGA^3$	0.1348415+ 0.02242434$\times US_MGA$	0.494875
EDVWR	1.043854-3.188297E-07$\times BPD^3$+ 1.095675E-07$\times LN(BPD) \times BPD^3$	0.1314646+ 0.0004215957$\times EFW$	0.037178	1.052541-0.0004567135$\times LMP_GA^2$+ 0.0001549685$\times LN(LMP_GA) \times LMP_GA^2$	0.1272925+ 0.001224838$\times LMP_GA$	0.035548
EDVLR	0.9469599+940.4648$/BPD^2$- 278.9847$\times LN(BPD)/BPD^2$	0.05387099+ 0.0001789679$\times BPD$	0.009917	0.9543317+20855.35$/HC^2$- 4437.48$\times LN(HC)/HC^2$	0.05202518+ 5.71136E-05$\times HC$	0.009528
EDVAR	-10.4032+2.235013$\times LN(LMP_GA)$+ 20.42147$/\sqrt{LMP_GA}$	0.07003652+ 0.003342709$\times LMP_GA$	0.058119	0.8482351-1.873583E-08$\times AC^3$+ 4.139678E-09$\times LN(AC) \times AC^3$	0.08761315+ 0.0003215126$\times AC$	0.055427

Table S11: Regression function of the Z-score modeling for cardiac parameters of left heart structures. $1st$ and $2nd$ formulation are the two with the highest correlation coefficients R^2.

Function	$1st$ Formulation			$2nd$ Formulation		
Parameter	Mean	SD	R^2	Mean	SD	R^2
LAA	-1.864674+0.0002323954$\times EFW$+ 0.3701066$\times LN(EFW)$	0.05902709+ 0.0001061064$\times EFW$	0.795790	-3.763087+0.2983405$\times\sqrt{AC}$+ 10529.62$/AC^2$	-0.153187+ 0.001485108$\times AC$	0.788152
LVFAC	39.56292-6474919$/EFW^2$+ 1261084$\times LN(EFW)/EFW^2$	7.603603- 0.000573232$\times EFW$	0.082840	52.94372-7.775006E-06$\times HC^3$+ 1.280595E-06$\times LN(HC)/HC^3$	9.300826- 0.009558083$\times HC$	0.082698
LVTWd	2.104454+21.81886$/\sqrt{EFW}$- 8.621264$\times/\sqrt{EFW}$	0.06046021+ 3.641593E-05$\times EFW$	0.775077	3.459365-19.49643$/\sqrt{FL}$+ 566.3431$/FL^2$	-0.007745745+ 0.002286092$\times FL$	0.767287
LVSV	-0.09705434+0.0007898033$\times EFW$- 1.007181E-07$\times EFW^2$	0.003772123+ 0.0001696602$\times EFW$	0.717146	-2.255069+0.09636083$\times US_MGA$+ 198.2682$/US_MGA^2$	-0.4278197+ 0.02338353$\times US_MGA$	0.712084
LVEF	51.14313-7230606$/EFW^2$+ 1352585$\times LN(EFW)/EFW^2$	9.71603- 0.0006211709$\times EFW$	0.027803	43.28611-81728.89$/FL^2$+ 27398.28$\times LN(FL)/FL^2$	11.51061- 0.05197299$\times FL$	0.027517
LVCO	-76.89915+5.218984$\times\sqrt{EFW}$+ 540870$/EFW^2$	1.039452+ 0.02485917$\times EFW$	0.703983	-450.041+15.50245$\times US_MGA$+ 3329.796$/US_MGA$	-63.97472+ 3.497176$\times US_MGA$	0.698046
LVAVFS	18.03511-6262256$/EFW^2$+ 1233326$\times LN(EFW)/EFW^2$	6.224594- 0.0004536017$\times EFW$	0.127092	33.32545-9.915703E-06$\times HC^3$+ 1.644577E-06$\times LN(HC)\times HC^3$	7.577169- 0.007588991$\times HC$	0.126849
LVSI	-19.58081+2.144752$\times\sqrt{LMP_GA}$+ 65.19614$/\sqrt{LMP_GA}$	0.7435363- 0.002036999$\times LMP_GA$	0.056092	22.44665-4.128972$\times\sqrt{HC}$+ 0.5379816$\times LN(HC)\times\sqrt{HC}$	0.7663993- 0.0003106778$\times HC$	0.053447
LVGLS	19.35991-8279140$/EFW^2$+ 1585953$\times LN(EFW)/EFW^2$	6.267397- 0.0006578839$\times EFW$	0.142387	-33.91226+8.186756E-06$\times HC^3$- 1.347065E-06$\times LN(HC)\times HC^3$	8.49406- 0.01202862$\times HC$	0.136699
LVSWS	16.58337-8325934$/EFW^2$+ 1591830$\times LN(EFW)/EFW^2$	6.574865- 0.0005326542$\times EFW$	0.124252	31.35208-8.602259E-06$\times HC^3$+ 1.419058E-06$\times LN(HC)\times HC^3$	8.223259- 0.009077882$\times HC$	0.119487
LVFWS	21.36914-8321668$/EFW^2$+ 1596709$\times LN(EFW)/EFW^2$	6.880087- 0.0005655412$\times EFW$	0.120511	35.57092-7.490345E-06$\times HC^3$+ 1.226546E-06$\times LN(HC)\times HC^3$	8.814709- 0.01044095$\times HC$	0.116180
LVAPSE	0.8067635+2.994506E-08$\times EFW^2$- 6733.503$/EFW^2$	0.1998453+ 4.409313E-05$\times EFW$	0.056922	0.7607937-31.1362$/FL^2$+ 7.510771E-07$\times FL^3$	0.1290826+ 0.002462323$\times FL$	0.053036
LASID	-1.378879+0.342969$\times LN(EFW)$+ 3888.696$/EFW^2$	0.09853287+ 3.729149E-05$\times EFW$	0.642046	2.55602-482.6301$/AC$+ 29319.35$/AC^2$	0.02009236+ 0.0005392848$\times AC$	0.636711
LATD	1.037539+0.01025639$\times\sqrt{EFW}$- 10.9819$/\sqrt{EFW}$	0.07683164+ 4.737692E-05$\times EFW$	0.715049	1.835497-24.38423$/US_MGA$+ 4.781249E-06$\times US_MGA^3$	-0.0387247+ 0.006387036$\times US_MGA$	0.707669
LVTWs	-1.179238+0.2971133$\times LN(EFW)$- 0.6119201$/\sqrt{EFW}$	0.06442285+ 3.430247E-05$\times EFW$	0.755497	2.647384-9.523871$/\sqrt{US_MGA}$+ 2.508526E-06$\times US_MGA^3$	-0.02013893+ 0.004691022$\times US_MGA$	0.745502
LVBALd	-1.935251+0.5849769$\times LN(EFW)$+ 1.648718E-08$\times EFW^2$	0.1281248+ 5.164431E-05$\times EFW$	0.794829	3.239918-36.78759$/US_MGA$+ 1.353233E-05$\times US_MGA^3$	-0.01037544+ 0.00753454$\times US_MGA$	0.785727
LVBALs	-2.127574+0.5517424$\times LN(EFW)$+ 4.666385E-09$\times EFW^2$	0.1258557+ 4.190002E-05$\times EFW$	0.785410	4.781376-16.59559$/\sqrt{US_MGA}$+ 6.133472E-06$\times US_MGA^3$	0.0181997+ 0.005957071$\times US_MGA$	0.778245
LVEAd	-1.231011+0.1707085$\times\sqrt{EFW}$- 0.01131768$\times LN(EFW)\times\sqrt{EFW}$	0.07271678+ 0.0001721229$\times EFW$	0.848388	-2.562575+0.1548183$\times US_MGA$+ 85.63237$/US_MGA^2$	-0.3512512+ 0.02342422$\times US_MGA$	0.840064
LVEAs	-7.959069+1.164039$\times LN(EFW)$+ 28.57653$/\sqrt{EFW}$	0.05666393+ 0.0001181835$\times EFW$	0.814081	-5.718359+1.228674$\times\sqrt{US_MGA}$+ 249.8127$/US_MGA^2$	-0.2360179+ 0.01608048$\times US_MGA$	0.804560
LVEVd	-1.40173+0.07673393$\times\sqrt{EFW}$+ 88.60889$/EFW$	-0.0215361+ 0.00028565$\times EFW$	0.803738	-1.139387+0.002939291$\times US_MGA^2$+ 106.6378$/US_MGA^2$	-0.7244621+ 0.03857394$\times US_MGA$	0.795988
LVEVs	-1.026736+0.04178512$\times\sqrt{EFW}$+ 6.875035$/\sqrt{EFW}$	-0.009578485+ 0.0001594203$\times EFW$	0.751875	14.04923+0.8672236$\times\sqrt{AC}$- 4.90218$\times LN(AC)$	-0.3094566+ 0.002140061$\times AC$	0.742658
LVECLd	-4.283714+1.238747$\times LN(EFW)$+ 2.116746E-08$\times EFW^2$	0.2707162+ 0.0001206016$\times EFW$	0.781833	10.98326-36.2709$/\sqrt{US_MGA}$+ 1.713075E-05$\times US_MGA^3$	-0.04424353+ 0.01711873$\times US_MGA$	0.773887
LVECLs	-4.805037+1.177782$\times LN(EFW)$+ 7457.801$/EFW^2$	0.2510267+ 8.812646E-05$\times EFW$	0.789940	9.510801-219.3652$/\sqrt{US_MGA}$+ 1457.288$/US_MGA^2$	0.01725396+ 0.01273978$\times US_MGA$	0.782419
LVECSWLd	-1.759665+0.5340366$\times LN(EFW)$+ 1.018805E-08$/EFW^2$	0.1378999+ 6.58752E-05$\times EFW$	0.712637	4.798156-15.54201$/\sqrt{US_MGA}$+ 7.736725E-06$\times US_MGA^3$	-0.03875419+ 0.009483493$\times US_MGA$	0.706177
LVECSWLs	3.581948+41.33902$\times\sqrt{EFW}$- 15.20938$\times LN(EFW)/\sqrt{EFW}$	0.1361416+ 5.194338E-05$\times EFW$	0.714179	4.290547-96.4124$/US_MGA$+ 629.724$/US_MGA^2$	-0.007798248+ 0.007642954$\times US_MGA$	0.709171
LVECFWLd	-2.534355+0.7080868$\times LN(EFW)$+ 1.005732E-08$\times EFW^2$	0.1501488+ 5.76109E-05$\times EFW$	0.801142	6.269032-21.04761$/\sqrt{US_MGA}$+ 8.891295E-06$\times US_MGA^3$	-0.00523879+ 0.008453011$\times US_MGA$	0.792016
LVECFWLs	-2.747917+0.656165$\times LN(EFW)$+ 4591.647$/EFW^2$	0.1350555+ 4.777817E-05$\times EFW$	0.800316	7.71112-32.96173$/\sqrt{US_MGA}$+ 324.4688$/US_MGA^2$	0.009949803+ 0.00685514$\times US_MGA$	0.791045
LVFWd	-1.94987+0.6712464$\times LN(EFW)$+ 2.807463E-08$\times EFW^2$	0.293426+ 0.000105938$\times EFW$	0.530669	-4.663753+2.20583$\times LN(US_MGA)$+ 7.179089E-06$\times US_MGA^3$	-0.003075026+ 0.01558971$\times US_MGA$	0.526451

Table S12: Regression function of the Z-score modeling for cardiac parameters of right heart structures. $1st$ and $2nd$ formulation are the two with the highest correlation coefficients R^2.

Function Parameter	$1st$ Formulation			$2nd$ Formulation		
	Mean	SD	R^2	Mean	SD	R^2
RAA	-0.3572807+0.04004366$\times\sqrt{EFW}$+ 4.208402E-08$\times EFW^2$	0.03190455+ 0.0001535882$\times EFW$	0.814262	-0.09264535+1.989652E-05$\times AC^2$+ 2.641765E-09$\times AC^3$	-0.2469261+ 0.002005378$\times AC$	0.807418
RVFAC	26.85739+8744.73/EFW- 1420705/EFW^2	7.565372- 5.923737E-05$\times EFW$	0.141473	12.51655-6930528/HC^2+ 1504499$\times LN(HC)/HC^2$	8.079425- 0.002277671$\times HC$	0.137802
RVTWd	-1.409063+5.166557E-05$\times EFW$+ 0.3396737$\times LN(EFW)$	0.06103806+ 4.206478E-05$\times EFW$	0.816456	-2.920393+1.168258$\times LN(US_MGA)$+ 3.725983E-06$\times US_MGA^3$	-0.04932328+ 0.005991498$\times US_MGA$	0.810657
RVAVFS	19.30026-8057394/EFW^2+ 1534616$\times LN(EFW)/EFW^2$	5.861246- 0.0002821175$\times EFW$	0.126546	32.20997-6.792953E-06$\times HC^3$+ 1.112793E-06$\times LN(HC) \times HC^3$	7.21751- 0.006796125$\times HC$	0.121169
RVSI	3.037076+27271.18/HC^2- 2.955429E-09HC^3	0.7739113- 0.001226816$\times HC$	0.148996	3.042126+1962.96/BPD^2- 1.01433E-07$\times BPD^3$	0.7625516- 0.004301276$\times BPD$	0.148180
RVGLS	20.84051-7635953/EFW^2+ 1463751$\times LN(EFW)/EFW^2$	5.571939- 0.0002374645$\times EFW$	0.138868	-34.36928+7.615768E-06$\times HC^3$- 1.253053E-06$\times LN(HC) \times HC^3$	6.773313- 0.006024112$\times HC$	0.134584
RVSWS	17.05642-6534083/EFW^2+ 1280658$\times LN(EFW)/EFW^2$	5.768949- 0.0002413921$\times EFW$	0.143228	39.09654-0.002691753$\times HC^2$+ 0.0004306542$\times LN(HC) \times HC^2$	6.814411- 0.00537617$\times HC$	0.140078
RVFWS	23.60241-8732073/EFW^2+ 1650367$\times LN(EFW)/EFW^2$	6.436565- 8.693667E-05$\times EFW$	0.100925	36.41004-6.497086E-06$\times HC^3$+ 1.062016E-06$\times LN(HC) \times HC^3$	7.23132- 0.003663613$\times HC$	0.096183
RVAPSE	0.7880683-90.95603/FL^2+ 6.920215E-07$\times FL^3$	0.07450105+ 0.003255003$\times FL$	0.080646	0.7946627-42.88253/LMP_GA^2+ 4.907084E-06$\times LMP_GA^3$	0.02426561+ 0.007770367$\times LMP_GA$	0.079200
RASID	-1.157976+0.3108289$\times LN(EFW)$+ 2.186158E-08/EFW^2	0.06608526+ 4.652174E-05$\times EFW$	0.769718	0.8503488-0.3490542$\times\sqrt{AC}$+ 0.06635446$\times LN(AC) \times SQRT(AC)$	-0.01992084+ 0.0006209756$\times AC$	0.762465
RATD	-1.451434+0.3553153$\times LN(EFW)$+ 1.998109E-08$\times EFW^2$	0.06777557+ 4.768635E-05$\times EFW$	0.795061	-1.671299+0.1753957$\times\sqrt{AC}$+ 2967.237/AC^2	-0.02244589+ 0.0006383422$\times AC$	0.791596
RVTWs	-2.395295+0.4766208$\times LN(EFW)$+ 53.63906/EFW	0.05775741+ 4.479528E-05$\times EFW$	0.831263	3.985664+1521.902/AC- 407.3315$\times LN(AC)/AC$	-0.02296701+ 0.0005859619$\times AC$	0.824349
RVBALd	-1.839707+0.5401441$\times LN(EFW)$+ 1.661831E-08$\times EFW^2$	0.1278437+ 3.287823E-05$\times EFW$	0.806890	-3.975837+1.761879$\times LN(US_MGA)$+ 5.058127E-06$\times US_MGA^3$	0.02439321+ 0.005335943$\times US_MGA$	0.799595
RVBALs	-2.264194+0.5422686$\times LN(EFW)$+ 7107.395/EFW^2	0.1166091+ 2.681256E-05$\times EFW$	0.803664	-5.719623+2.146721$\times LN(US_MGA)$+ 109.1453/US_MGA^2	0.04178718+ 0.00406925$\times US_MGA$	0.796922
RVEAd	-0.6108732+0.06573961$\times\sqrt{EFW}$+ 2.456326E-08$\times EFW^2$	0.07045977+ 0.0001513899$\times EFW$	0.877883	-2.302837+0.5853593$\times\sqrt{US_MGA}$+ 4.038513E-05$\times US_MGA^3$	-0.3360471+ 0.02186715$\times US_MGA$	0.869631
RVEAs	-0.6741487+0.05225725$\times\sqrt{EFW}$+ 7355.056/EFW^2	0.0441048+ 0.0001214548$\times EFW$	0.861933	4.886857+0.2174811$\times US_MGA$- 2.95697$\times LN(US_MGA)$	-0.2894053+ 0.01788142$\times US_MGA$	0.853891
RVECLd	-3.401776+0.000222163$\times EFW$+ 1.01673$\times LN(EFW)$	0.2538517+ 7.524191E-05$\times EFW$	0.822614	-7.986457+3.514159$\times *LN(US_MGA)$+ 1.503531E-05$\times US_MGA^3$	0.03305888+ 0.01167436$\times US_MGA$	0.816168
RVECLs	-4.908931+1.135068$\times LN(EFW)$+ 16967.08/EFW^2	0.2198554+ 6.017586E-05$\times EFW$	0.822589	13.84215-61.75731/$\sqrt{US\_MGA}$+ 749.9282/US_MGA^2	0.03403488+ 0.009744025$\times US_MGA$	0.816823
RVECSWLd	-1.560915+0.472927$\times LN(EFW)$+ 1.849755E-08/EFW^2	0.118579+ 4.757512E-05$\times EFW$	0.758174	4.028331-12.88484/$\sqrt{US\_MGA}$+ 9.875425E-06$\times US_MGA^3$	-0.007694751+ 0.006849721$\times US_MGA$	0.751387
RVECSWLs	-1.705359+0.4459418$\times LN(EFW)$+ 1.052153E-08$\times EFW^2$	0.1033403+ 3.900374E-05$\times EFW$	0.780590	-3.535918+1.479227$\times LN(US_MGA)$+ 3.259253E-06$\times US_MGA^3$	0.001755043+ 0.005517259$\times US_MGA$	0.774622
RVECFWLd	-2.074261+0.000132008$\times EFW$+ 0.5898509$\times LN(EFW)$	0.1492749+ 4.896719E-05$\times EFW$	0.812947	-4.729778+2.036987$\times LN(US_MGA)$+ 8.962827E-06$\times US_MGA^3$	0.0005216611+ 0.007754346$\times US_MGA$	0.807089
RVECFWLs	-2.911349+0.6472114$\times LN(EFW)$+ 12299.39/EFW^2	0.1323829+ 4.645205E-05$\times EFW$	0.782789	5.22602-136.4886/US_MGA+ 1037.531/US_MGA^2	-0.006835736+ 0.00733029$\times US_MGA$	0.777585
RVFWd	-2.20175+0.7193741$\times LN(EFW)$+ 2.731639E-08$\times EFW^2$	0.2137716+ 0.0001693162$\times EFW$	0.559621	-13.54974+2.959407$\times LN(AC)$+ 15544.05/AC^2	-0.09511662+ 0.002210211$\times AC$	0.557271